DISTRIBUTED FIBER-OPTIC STRAIN AND TEMPERATURE SENSORS USING PHOTOINDUCED BRAGG GRATINGS

by

Mark E. Froggatt

Thesis submitted to the Faculty of the
Virginia Polytechnic Institute and State University
in partial fulfillment of the requirements for the degree of
MASTER OF SCIENCE
in
Electrical Engineering

APPROVED:

Richard O. Claus

Dr. R. O. Claus, Chairman

Dr. D. A. deWolf

Dr. K. A. Murphy

February, 1995
Blacksburg, Virginia

DISTRIBUTED FIBER-OPTIC STRAIN AND TEMPERATURE SENSORS USING PHOTOINDUCED BRAGG GRATINGS

by

Mark E. Froggatt

Dr. R. O. Claus, Chairman

Electrical Engineering

Abstract

Much of the analytical and computational work necessary for the development of distributed fiber-optic strain sensors using photo induced Bragg gratings is presented. The one dimensional wave equation is solved for a slowly varying sinusoidal modulation of the index of refraction. The solution is found to take the form of a fourier transform for low reflectivity (<15%) gratings. As a result, the process can be inverted, and if the phase and amplitude of the reflected light can be measured over frequency, the phase and amplitude of the bragg grating as a function of length can be computed using the inverse fourier transform. These results are computationally verified, and then further analysis of critical engineering parameters is carried out. A measurement system and procedure are described. A method of writing long, low-reflectivity bragg grating is proposed.

Table of Contents

List of Figures

depths at each writing wavelength are assumed to be equal.

Figure 20. Experimental set-up to measure the vector reflection spectrum of a Bragg grating.

I. Introduction

Since 1990, there has been increasing interest in Bragg gratings for applications in both communications, and fiber optic sensors. Bragg gratings result when germanium doped optical fibers are exposed to light which has an intensity that varies periodically along the core of the fiber. A reaction at oxygen vacancy centers of the germanium dopant results in small changes in the index of refraction as a function of the local light intensity. The periodic change in the index of refraction along the core causes mode coupling between the forward and backward traveling modes of light in the fiber. This coupling is strong only when the wavelength of the light is an even multiple of the period of the perturbation of the index of refraction.

An examination of the literature reveals that most methods of interrogating Bragg gratings involve the determination of the center frequency of the grating. These methods discard the information available from the entire spectral response of the Bragg grating. The goal of this work is to provide the theoretical and computational means of extracting this information. An additional goal is to provide much of the analysis that will be necessary in order to construct the system that will measure the spectral response of the in-fiber Bragg grating.

In this work, I will develop a means of computing the spectral response of an arbitrary grating. This grating will be arbitrary in the sense that the phase and amplitude of the index of refraction modulation may be determined by a slowly varying complex function. By slowly varying, I mean that they do not change significantly within a period of the grating. Since the slowly varying function will be complex, any distortions of the

grating can be modeled. A significant limitation of the computational model developed is that it does not converge for high reflectivity gratings, which is not of great concern for sensing applications. However, high reflectivity filters are desirable to the communications industry, where I believe that this work could also be important. In this case, additional work on the computational methods is necessary.

After developing the theory and software necessary to compute the spectral response of a Bragg grating, I will then develop the theory and computational methods necessary to reconstruct the grating from the spectral response. In doing so I will make a stationary phase approximation under somewhat questionable circumstances. Since no such approximation was necessary in the spectral response computation, and since I will have the original grating description available, the effects of the stationary phase approximation can be readily studied.

The methods developed here could be used in multiple applications. An early application may be as a means of measuring the effects of the optical system used to write the gratings when side illumination is used. Since the beams used to write these gratings are gaussian beams, it would be expected that the envelopes of most gratings written with these beams would also be gaussian. When intervening optics are used, such as cylindrical lenses, this envelope may be distorted. The methods developed here would allow such effects to be measured directly.

A second application that could be important to nondestructive evaluation would be the development of localized distributed sensors. By mapping out distortions of the Bragg grating, strain over the length of the grating could be mapped out with the resolution determined primarily by the laser interrogating the grating. Figure 1 gives a pictorial representation

of the distributed sensor. Strain within the fiber causes changes in the periodicity of the grating. This change in periodicity can be measured as a constantly increasing phase shift in the slowly varying modulation of the grating. Figure 2 is an example of how strain as a function of length might be displayed. Longer gratings, written by standing waves (Hill gratings), could be used to produce distributed strain sensors over several meters of optical fiber.

In order to generate long gratings in coated fibers, I will propose a method relying upon the nonlinear nature of the change in the index of refraction. This method will use low germanium doping levels in the fiber core. A difference frequency will be generated from two standing waves around 488nm to produce a grating that will be reflective at 1300nm.

Because both phase and amplitude information are necessary to compute the grating structure, a vector spectrum analyzer is needed that will operate around a telecommunications wavelength (i.e. 1300nm). A tunable laser will be used as the source, and a balanced, PZT modulated Michelson interferometer will be used as the receiver. This system will be designed and analyzed to determine specifications for the distributed sensor. Specifications such as strain resolution, maximum length, distance resolution and speed of measurement will be computed.

II. Review of the Literature

Writing Bragg Gratings

The first Bragg grating was written in 1978 [1]. It was written by a standing wave pattern set up inside an optical fiber by counter propagating 488nm light from an argon laser. Exposure time for a 250mW laser was in the "tens of minutes," and gratings could only be written at the wavelength of the laser used to write them. The Hill method, as it came to be called after its inventor, does have two advantages over later, more flexible methods. The first advantage is that the Hill method did not require that the buffer be stripped from the fiber, and thus the fiber was saved from exposure to atmospheric moisture. An additional advantage was that long gratings (1m) were written. This characteristic is generally regarded as a disadvantage in communications applications since it results in an extremely narrow bandwidth. For the application to be discussed here, however, the ability to produce long gratings is an important capability.

Lam and Garside published a more detailed study of these gratings generated by standing waves [2]. Using the same experimental setup as in Hill's original work, Lam and Garside studied the effects of writing power on the gratings generated. Each grating was written until the reflectance saturated, and then the fiber grating was cut progressively shorter. By measuring the reflectance of the grating after each cut, a plot of the reflectance versus length could be made. Given the reflectance and the length of a grating, the modulation of the index of refraction can be calculated. It was found that the modulation of the index of refraction increased as the square of the writing power. This

result was viewed as support for the two photon theory of the photosensitivity phenomenon. Lam and Garside calculated index of refraction modulations as large as 200ppm when 140mW was the power of the writing laser.

A second method of writing fiber-optic Bragg gratings followed the discovery that the method used by Hill involved a two-photon reaction at 488nm, and that 244nm light would provide dramatic gains in efficiency for the process [3]. The new method, developed in 1989, wrote the grating into the core of the fiber by side exposing the fiber to an interference pattern generated by two coherent beams of 244nm light from an eximer laser. In this case, the light was introduced to the core through the cladding from the side of the fiber. The period of the interference fringe was dependent upon the angle of the intersection, so gratings could be written over a wide range of wavelengths. This holographic method has two principle disadvantages. The first is that in order to allow the UV light to enter the side of the fiber the buffer coating must be removed, thus exposing the glass to atmospheric moisture and embrittling it. The second is that the beam alignment must be precisely controlled during the period of exposure.

Hill devised a second means of writing gratings into fiber using side illumination [4]. This method wrote the grating one point at a time by exposing the fiber to UV radiation through a slit and carefully advancing the fiber to expose the next point to be written. This method required very precise mechanical control of the fiber positioning, and has not been widely reproduced. This method would permit the writing of custom gratings, with custom blaze angles and custom periodicity. Both of these capabilities could be important to the developement of all-fiber "extrinsic" sensors due to the ability of angled gratings to couple light in and out of the fiber core.

A third method devised by Hill of writing in-fiber Bragg gratings has found wide acceptance [5]. This method uses a holographic phase mask with a period that produces the desired interference pattern in the core of the fiber. This method is not as demanding of alignment precision as the previously mentioned side illumination methods.

Two methods of enhancing the photosensitivity of the fiber have been developed. The most widely used, and least documented method involves a process called "hydrogen loading." In this process, stripped optical fiber is placed in a hydrogen atmosphere at 2000 psi and elevated to a temperature of 70 C [6]. This process only accelerates the writing time, and does not result in larger index of refraction changes. The obvious safety aspects of this process usually have restricted its use to places with the necessary facilities.

Another way to enhance the photosensitivity of optical fiber is to co-dope germanium core fiber with boron [7]. This results in an estimated tenfold reduction in the necessary writing time, and an increase in the maximum change in the index of refraction to 20 times the value of standard telecommunications fiber. The authors speculate that "the addition of boron to the core of the fibre [sic] enhances the densification contribution to the induced refractive index ...".[7] The D. L. Williams paper [7] reporting the results with boron co-doping, also reported a saturated index modulation of 34 ppm for standard germanium doped telecommunications fibers. This result conflicts with the 200ppm modulation reported by Lam and Garside. These two measurements of the saturated index of refraction modulation were obtained using different exposure methods (i.e. intracore standing waves at 488nm, and side exposure to an interference pattern at 244nm), but current theories concerning the

mechanism of the index of refraction change would not predict such a difference in the results.

In review, there are currently four distinct methods of writing in-fiber Bragg gratings. The only method that couples light into the end of the fiber is the Hill or standing wave method, and this method can be used to write gratings only at the wavelength of the laser used to produce the grating. A second method is side exposure through the cladding to the interference pattern of two coherent beams of 244nm UV light. The third method uses side exposure through a phase mask placed on the fiber to produce an interference pattern. The fourth method exposes each point change in the index of refraction separately through a slit as the position of the fiber beneath the slit is mechanically advanced. All of the side exposure methods have the advantage of being somewhat tunable, and the point-by-point method has the additional advantage of offering the potential for custom gratings.

There are currently two methods of enhancing the photosensitivity of germanium-doped optical fiber. Both offer shorter writing times, and thus relaxed tolerances on the long term stability of the writing set up. Hydrogen loading has certain demonstrated safety problems associated with it (the bomb effect), while boron codoped fiber must be custom made. Boron codoping has the additional advantage of increasing the maximum index of refraction modulation.

Analysis of Bragg Gratings

There has been a significant amount of analysis done on Bragg gratings. The principle work was done prior to the development of Bragg gratings in 1978, and pertained to the general one dimensional problem of waves propagating in media

in which the wave number changes as a function of distance. Hill published a relatively complete analysis of the problem in 1974 [8]. At the time, he was analysing the problem of a corrugated two dimensional waveguide. However, many of the results match those derived here, and later served as a basis for Hill's further work. In this 1974 paper, Hill derives the same integral equations produced here, applies a similar stationary phase approximation to a chirped grating, and notes the resemblance of the reflection spectrum to the Fourier transform of the grating. Hill also notes that the iterative numerical solution to the pair of integral equations does not converge in some cases. He does not identify the circumstances of convergence.

Another 1974 paper by Matsuhara and Hill looks at the effects of modulating the amplitude of the index of refraction change [9]. They apply this effect to the reduction of sidelobes in the reflected spectrum of periodic optical filters. The analysis and results resemble the use of windowing in digital signal processing. This characteristic can be attributed to the Fourier transform relationship between the grating and the reflected spectrum.

Lam and Garside published a brief analysis of the spectral response of an in-fiber Bragg grating as an appendix to their largley experimental paper [2]. Their analysis finds the differential equations associated with Bragg gratings, and then solves the for the case of a constant amplitude and phase grating of length L.

Bernardin and Lawandy have analysed the formation of Bragg gratings using the Hill method of standing waves [10]. This analysis models the dynamic system involved in the formation of Bragg gratings. The current theories concerning the exact mechanism of the index of refraction change were discussed, and the equations describing the dynamic growth of gratings in a fiber

were derived based upon one of these mechanisms. These equations were then numerically solved for a number of simple cases.

In summary, the forward problem of calculating the spectral response given the grating has been analysed in a number of publications. However the solutions have generally been restricted to a few well defined grating structures, and no generalized procedure or algorithm has been developed. The reverse problem, that of finding the grating given the spectral response, has not been addressed in the literature. The analysis of the growth of standing wave generated gratings could become important in the creation of long gratings at common telecommunications wavelengths.

Bragg Grating Sensors

Strain sensors using Bragg gratings can be divided into two groups: those using broadband illumination, and those using in-fiber lasers. In both cases the demodulation problem is simply a wavelength measurement problem. The in-fiber laser systems have the advantage of comparatively high power levels, and thus allow faster or higher resolution measurement of the wavelength.

Melle et al. built a system that used an erbium doped fiber for the gain medium, and Bragg grating sensor as the output side of the fiber cavity, and a silver nitrate mirror on the other end of the fiber cavity [11]. The system was pumped at 980nm, and lased at 1550nm. The use of an end mirror, and the location of the erbium doped fiber outside of the test section avoided tracking problems that occur if Bragg grating sensors are used as both end faces of the cavity. The large cavity length, however meant that there was a large number of supported modes within the cavity.

Ball et al. describe a system using in-fiber lasers that utilize Bragg gratings for both ends of the fiber cavity [12]. Despite the shorter (3cm) laser cavity, this system also displayed mode-hopping problems. This configuration does have the advantage of permitting multiple sensors in a single fiber, and suffers from the requirement that the gratings at each end of the fiber track one another closely.

Bullock et al. built a system that used a simple white light interrogation system with a spectrum analyzer to measure strain through the thickness of a composite with an embedded Bragg grating [13]. A reference grating was incorporated in the same fiber and the measurement was made by comparing the sensing gratings resonant frequency to the reference grating's resonant frequency. Resolutions in the tens of microstrains were reported.

Morey et al. reviewed and analyzed a number of ways to multiplex Bragg grating sensors [14]. They analyzed two types of Bragg grating sensors. One was a single grating with wavelength readout, and the second was a pair of gratings forming a fabry perot interferometer in the fiber. Both time division multiplexing and wavelength division multiplexing were considered. No detailed computations were done, and no experimental results were reported.

Morey et al. describe the first holographically written Bragg gratings, and described their applications as sensors [15]. The response of Bragg gratings to temperature and strain was described, and experimental data was presented. An upper limit to the operating temperature of Bragg gratings was given to be around 500 C. Standard single grating sensor and Fabry-Perot sensor configurations were discussed.

Kersey et al. described an interferometric means of measuring dynamic shifts in the wavelength of the Bragg grating [16]. An unbalanced Michelson interferometer with PZT control of the unblanced arm length is used to detect small shifts in the wavelength of the grating. Lower frequency stability is achieved by using a reference grating isolated from the strain being measured. This method is applicable only to tracking dynamic or pseudo static strains.

In summary, two intrafiber laser methods of demodulation were discussed. One method uses Bragg gratings for both reflectors and places the gain medium within the sensor, and the other method uses a sensing Bragg grating as one reflector and a mirror as the other with the gain medium located outside of the sensing region. Using Bragg gratings for each sensor allows for multiplexed systems but introduces the tracking requirement between the gratings. The single grating method eliminates the tracking problem, and reduces the cost of the sensor, but does not permit multiplexing. A possibility not examined would be to place the gain medium within a grating, which could potentially eliminate both the tracking and the mode hopping problems.

The passive Bragg grating demodulation schemes consist of either an absolute determination of wavelength, or a wavelength tracking scheme. The tracking scheme has the obvious disadvantage that static strains are difficult or impossible to measure, and absolute methods have the disadvantage of requiring a spectrum analyzer to make the measurement. The resolution of some of these measurements has been enhanced by creating a Fabry-Perot cavity between two reflectors.

All of the demodulation methods described above assume that the spectral response of a grating can be characterized by a

single wavelength and reflectance. Non-uniform strain of the grating is not considered.

III. Theory

If nonuniform strains within the grating are to be considered, the grating must be analyzed with an arbitrary structure. The structure will be arbitrary in both phase and amplitude, and will permit the characterization of any slowly varying grating.

I begin with the one dimensional wave equation describing light propagating in the fiber along the x-axis. The index of refraction of the core varies as a function of x, and is expressed as a small modulation of the relative permittivity, $\varepsilon_r(x)$, giving,

$$\frac{\partial^2 E}{\partial x^2} + \beta^2(1+\varepsilon_r(x))E = 0 \quad (1)$$

The electric field, E, is assumed to consist of two fields propagating in opposite directions along the x-axis. Each field has a slowly varying complex amplitude. The electic field is then,

$$E = f(x)e^{j\beta x} + g(x)e^{-j\beta x}. \quad (2)$$

Taking the second derivative of the electric field with respect to x, gives,

$$\frac{\partial^2 E}{\partial x^2} = \frac{\partial^2 f}{\partial x^2}e^{j\beta x} + 2j\beta\frac{\partial f}{\partial x}e^{j\beta x} - \beta^2 f(x)e^{j\beta x} + \frac{\partial^2 g}{\partial x^2}e^{-j\beta x} - 2j\beta\frac{\partial g}{\partial x}e^{-j\beta x} - \beta^2 g(x)e^{-j\beta x}. \quad (3$$

Applying the slowly varying approximation, the second order derivatives of the electric field amplitudes are neglected and Eqn. (3) reduces to,

$$\frac{\partial^2 E}{\partial x^2} = 2j\beta\frac{\partial f}{\partial x}e^{j\beta x} - \beta^2 f(x)e^{j\beta x} - 2j\beta\frac{\partial g}{\partial x}e^{-j\beta x} - \beta^2 g(x)e^{-j\beta x} \quad . \qquad (4)$$

Substituting Eqn. (4) and Eqn. (2) into Eqn. (1), gives,

$$2j\beta(\frac{\partial f}{\partial x}e^{j\beta x} - \frac{\partial g}{\partial x}e^{-j\beta x}) - \beta^2\varepsilon_r(x)(f(x)e^{j\beta x} + g(x)e^{-j\beta x}) = 0 \quad . \qquad (5)$$

Since I will be interested in the response of the grating as a function of the wavelength of the incident light, I will allow the in-fiber wavenumber to change by a small amount, ξ, giving,

$$2j(\beta+\xi)(\frac{\partial f}{\partial x}e^{j(\beta+\xi)x} - \frac{\partial g}{\partial x}e^{-j(\beta+\xi)x}) + (\beta+\xi)^2\varepsilon_r(x)(f(x)e^{j(\beta+\xi)x} + g(x)e^{-j(\beta+\xi)x}) = 0 \quad .$$

(6)

I then represent the variation of the index of refraction as a cosine with a slowly varying modulation of the phase and amplitude, $\kappa(x)$

$$\varepsilon_r(x) = \kappa(x)e^{j2\beta x} + \kappa^*(x)e^{-j2\beta x} \quad . \qquad (7)$$

Substituting Eqn. (7) into Eqn. (6) gives,

$$0 = 2j(\beta+\xi)(\frac{\partial f}{\partial x}e^{j(\beta+\xi)x} - \frac{\partial g}{\partial x}e^{-j(\beta+\xi)x}) +$$
$$(\beta+\xi)^2(\kappa(x)e^{j2\beta x} + \kappa^*(x)e^{-j2\beta x})(f(x)e^{j(\beta+\xi)x} + g(x)e^{-j(\beta+\xi)x}) \quad . \qquad (8)$$

Multiplying out the last term yeilds,

$$0 = 2j(\beta+\xi)(\frac{\partial f}{\partial x}e^{j(\beta+\xi)x} - \frac{\partial g}{\partial x}e^{-j(\beta+\xi)x}) + (\beta+\xi)^2\kappa(x)f(x)e^{j(3\beta+\xi)x}$$
$$+(\beta+\xi)^2\kappa(x)g(x)e^{j(\beta-\xi)x} + (\beta+\xi)^2\kappa^*(x)f(x)e^{-j(\beta-\xi)x} + (\beta+\xi)^2\kappa^*(x)g(x)e^{-j(3\beta+\xi)x} \quad .$$

(9)

Since this must hold for all x, terms propagating in the same direction at nearly the same frequency can be matched to produce two coupled differential equations written as

$$2j(\beta+\xi)\frac{\partial f}{\partial x}e^{j(\beta+\xi)x}+(\beta+\xi)^2\kappa(x)g(x)e^{j(\beta-\xi)x}=0 \tag{10}$$

$$-2j(\beta+\xi)\frac{\partial g}{\partial x}e^{-j(\beta+\xi)x}+(\beta+\xi)^2\kappa^*(x)f(x)e^{-j(\beta-\xi)x}=0\ . \tag{11}$$

Rearranging,

$$\frac{\partial f}{\partial x}=\frac{(\beta+\xi)}{2j}\kappa(x)g(x)e^{-2j\xi x}\ , \tag{12}$$

$$\frac{\partial g}{\partial x}=-\frac{(\beta+\xi)}{2j}\kappa^*(x)f(x)e^{2j\xi x}\ . \tag{13}$$

These coupled differential equations, with $\kappa(x)=1$, appear in an article by Lam and Garside in 1981, and were solved for the case of $\kappa(x)=1$. If (12) and (13) are to be solved, further steps must be taken. I begin by integrating both sides, and choosing the limits of integration to provide us with known initial conditions. This operation gives,

$$\int_{-\infty}^{x}df=\frac{(\beta+\xi)}{2j}\int_{-\infty}^{x}\kappa(z)g(z)e^{-2j\xi z}dz \tag{14}$$

$$\int_{x}^{\infty}dg=-\frac{(\beta+\xi)}{2j}\int_{x}^{\infty}\kappa^*(z)f(z)e^{2j\xi z}dz\ . \tag{15}$$

Performing the integrations on the left we get,

$$f(x)-f(-\infty)=\frac{(\beta+\xi)}{2j}\int_{-\infty}^{x}\kappa(z)g(z)e^{-2j\xi z}dz\ , \tag{16}$$

$$g(\infty)-g(x)=-\frac{(\beta+\xi)}{2j}\int_{x}^{\infty}\kappa^*(z)f(z)e^{2j\xi z}dz\ . \tag{17}$$

Choosing the initial conditions such that there is light being transmitted from minus infinity, and assuming that there is no backward traveling light at plus infinity, gives

$$f(-\infty)=1, \tag{18}$$
$$g(\infty)=0. \tag{19}$$

This assumption then yields an expression for the amplitude and phase of the counter propagating fields. One should note at this point that both of these fields depend upon ξ as noted explicitly in,

$$f(x,\xi)=\frac{(\beta+\xi)}{2j}\int_{-\infty}^{x}\kappa(z)g(z,\xi)e^{-2j\xi z}dz+1, \tag{20}$$
$$g(x,\xi)=\frac{(\beta+\xi)}{2j}\int_{x}^{\infty}\kappa^{*}(z)f(z,\xi)e^{2j\xi z}dz. \tag{21}$$

$g(x,\xi)$ is evaluated at $x=-\infty$ to find the phase and amplitude of the back scattered light as a function of ξ giving,

$$g(-\infty,\xi)=\frac{(\beta+\xi)}{2j}\int_{-\infty}^{\infty}\kappa^{*}(z)f(z,\xi)e^{2j\xi z}dz. \tag{22}$$

Because this resembles a Fourier transform of $\kappa^{*}(z)$with $f(z,\xi)$ as a kernel, an inverse fourier transform of both sides is taken giving,

$$\int_{-\infty}^{\infty}g(-\infty,\xi)e^{-2j\xi z_0}d2\xi=\int_{-\infty}^{\infty}\frac{(\beta+\xi)}{2j}e^{-2j\xi z_0}\int_{-\infty}^{\infty}\kappa^{*}(z)f(z,\xi)e^{2j\xi z}dzd2\xi. \tag{23}$$

Changing the order of integration and neglecting the ξ in the $\beta+\xi$ term, since I have noted earlier that ξ will be a very small change in the wavenumber, gives,

$$\int_{-\infty}^{\infty} g(-\infty,\xi)e^{-2j\xi z_0}d\xi = \frac{\beta}{2j}\int_{-\infty}^{\infty}\int_{-\infty}^{\infty}\kappa^*(z)f(z,\xi)e^{2j\xi(z-z_0)}d\xi dz. \tag{24}$$

Substituting,

$$\omega = 2\xi, \text{ and} \tag{25}$$
$$d\omega = 2d\xi, \tag{26}$$

gives,

$$\int_{-\infty}^{\infty} g(-\infty,\frac{\omega}{2})e^{-j\omega z_0}\frac{1}{2}d\omega = \frac{\beta}{2j}\int_{-\infty}^{\infty}\int_{-\infty}^{\infty}\kappa^*(z)f(z,\frac{\omega}{2})e^{j\omega(z-z_0)}\frac{1}{2}d\omega dz. \tag{27}$$

In order to proceed, a stationary phase approximation must be used for $\kappa^*(z)$ and $f(z,\frac{\omega}{2})$. In this approximation, I assume that for values of z much different than z_0 there is little contribution to the integral due to the oscillation of the $e^{j\omega(z-z_0)}$ term. Clearly, this will not be true for small values of ω. Problems arising from this can be avoided by choosing β such that it is far off the grating resonance. We can then let the magnitude of $f(z,\frac{\omega}{2})$ be zero around $\omega = 0$. Making the approximation yields,

$$\int_{-\infty}^{\infty} g(-\infty,\frac{\omega}{2})e^{-j\omega z_0}d\omega = \frac{\beta}{2j}\int_{-\infty}^{\infty}\kappa^*(z_0)f(z_0,\frac{\omega}{2})e^{-j\omega z_0}\int_{-\infty}^{\infty}e^{j\omega z}dzdw. \tag{28}$$

Evaluating integrals gives,

$$2G(-\infty,2z_0) = \frac{\beta}{2j}\int_{-\infty}^{\infty}\kappa^*(z_0)f(z_0,\frac{\omega}{2})e^{-j\omega z_0}2\pi\delta(\omega)d\omega, \tag{29}$$

and using the sifting property of delta functions,

$$G(-\infty,2z_0)=\frac{\pi\beta}{2j}\kappa^*(z_0)f(z_0,0). \tag{30}$$

This equation is used in conjunction with the equations below, in which ξ has been set to zero, to form an iterative numerical method for finding $\kappa(x)$ given $g(-\infty,\xi)$.

$$f(z_0,0)=\frac{\beta}{2j}\int_{-\infty}^{z_0}\kappa(z)g(z,0)dz+1 \tag{31}$$

$$g(z_0,0)=\frac{\beta}{2j}\int_{z_0}^{\infty}\kappa^*(z)f(z,0)dz \tag{32}$$

A careful selection of β avoids the problems around $\omega=0$. If β is chosen far off resonance, then $g(z_0,0)=0$, and $f(z_0,0)=1$. This assumption guarantees that there is no significant variation with z_0 and reduces the system of three equations to

$$G(-\infty,2z_0)=\frac{\pi\beta}{2j}\kappa^*(z_0). \tag{33}$$

The computation of the grating structure given the reflection spectrum is thus reduced to a fourier transform. This reduction opens the possibility of realtime monitoring of Bragg gratings, since 1000 point transforms can now be performed in under one millisecond.

IV. Computational Work

Numerical Methods

For most of my computational work, I will use the integral forms of the equations. The algorithms were implemented in FORTRAN, and executed on a Convex computer. The spectral computations were the most computationally intensive, since each point required multiple (about 30) complex numerical integrations over1000 points. To find the spectral response of the grating, the system of equations in (15) must be solved for the spectral response of the Bragg grating.

$$f(x,\xi) = \frac{(\beta+\xi)}{2j}\int_{-\infty}^{x} \kappa(z) g(z,\xi) e^{-2j\xi z} dz + 1 \tag{34}$$

$$g(x,\xi) = \frac{(\beta+\xi)}{2j}\int_{x}^{\infty} \kappa^{*}(z) f(z,\xi) e^{2j\xi z} dz \tag{35}$$

Factoring out the maximum modulation of the index of refraction as m so that,

$$\max\left\{\frac{\kappa(z)}{m}\right\} = 1, \text{ and } m\mathrm{K}(z) = \kappa(z), \qquad (36)\ (37)$$

and neglecting the ξ in the $\beta+\xi$ factor gives

$$f(x,\xi) = \frac{\beta m}{2j}\int_{-\infty}^{x} \mathrm{K}(z) g(z,\xi) e^{-2j\xi z} dz + 1, \tag{38}$$

$$g(x,\xi) = \frac{\beta m}{2j}\int_{x}^{\infty} \mathrm{K}^{*}(z) f(z,\xi) e^{2j\xi z} dz. \tag{39}$$

Next, the integrals are converted to sums and written as,

$$f(n\Delta x,\xi) \cong 1 + \frac{\beta m}{2j}\sum_{i=1}^{n} \mathrm{K}(i\Delta x) g(i\Delta x,\xi) e^{-2j\xi i\Delta x}\Delta x, \tag{40}$$

$$g(n\Delta x,\xi) \cong \frac{\beta m}{2j}\sum_{i=1}^{n} \mathrm{K}^{*}(i\Delta x) f(i\Delta x,\xi) e^{2j\xi i\Delta x}\Delta x. \tag{41}$$

And now converting to discrete functions $\tilde{f}(n,\xi)$ and $\tilde{g}(n,\xi)$,

$$\tilde{f}(n,\xi) \cong 1 + \frac{\beta m}{2j}\sum_{i=1}^{n} \tilde{\mathrm{K}}(i) \tilde{g}(i,\xi) e^{-2j\xi i\Delta x}\Delta x \tag{42}$$

$$\tilde{g}(n,\xi) \cong \frac{\beta m}{2j}\sum_{i=1}^{n} \tilde{\mathrm{K}}^{*}(i) f(i,\xi) e^{2j\xi i\Delta x}\Delta x. \tag{43}$$

By making an initial guess of $\tilde{f}(n,\xi)=1$, Eqn. (41) and Eqn. (42) can be solved iteratively. For low reflectivity gratings, the process converges within 15 iterations. The important factor in this convergence will be referred to as the coupling factor, C.

$$C = \frac{\beta m N \Delta x}{2} = \frac{\pi L m}{\lambda_f} \tag{44}$$

where L is the length of the grating and λ_f is the in-fiber wavelength of the center frequency of the Bragg grating. If $C<1$ then the process will generally converge. If C is close to 1, sometimes the process will not converge. Values of C less than 0.75 guarantee rapid convergence.

If the spectral response is given and $\kappa(x)$ is desired, another computational algorithm is necessary. This time, the spectral response is given as,

$$\tilde{g}(-\infty,k) = g(-\infty,k\Delta\xi). \tag{45}$$

A Fast Fourier Transform of $\tilde{g}(-\infty,k)$ is taken and the result is substituted into (33) to give

$$\tilde{G}(-\infty,2k)=\frac{\pi\beta}{2j}\Delta x\tilde{K}^{*}(k). \tag{46}$$

Solving for $\tilde{K}^{*}(k)$,

$$\tilde{K}^{*}(k)=\frac{2j}{\pi\beta\Delta x}G(-\infty,2k). \tag{47}$$

The result is then a simple discrete Fourier transform of the measured spectral response. Since FFT engines are readily available, it is possible that an FFT of the spectral response could be computed in real time as the fiber was written, or as the fiber was strained on a structure.

Results of Numerical Analysis

The software implementing the algorithms described above has been written and tested. It is contained in two FORTRAN programs. REFLECT.F computes the reflection coefficients over a range of values of ξ from an input file containing $\tilde{K}(k)$. RECON.F reconstructs $\tilde{K}(k)$ from the spectral response computed by REFLECT.F. Recall that the algorithm for computing the spectral response required no approximations other than the slowly varying approximation, and therefore, the spectral response computed by it should be accurate. The algorithm for computing $\tilde{K}(k)$, however, required the stationary phase approximation.

Figure 3 shows a complicated modulation of the magnitude of the induced change in the index of refraction of the core as a function of length, and figure 4 shows the reconstructed modulation from the reflected spectrum. Note that on the right side of the reconstructed modulation the modulation valleys no

longer go to zero. This error is due to the stationary phase approximation. Figure 5 shows the computed magnitude of the spectral response of the original modulation grating shown in Figure 3.

Figures 6 and 7 show the original and the reconstructed abrupt rectangular modulations of the Bragg grating amplitude. Here, the errors due to the stationary phase approximation are more evident at the end of the grating. Figure 8 is the magnitude of the computed spectral response of the original abrupt rectangular grating.

Figures 9 and 10 show original and the reconstructed gaussian modulations. This is the sort of modulation that one would expect a gaussian laser beam to produce. Figure 11 shows the computed magnitude of the spectral response of original gaussian shown in Figure 9.

Figure 12 shows the computation of strain as a function of distance through a bragg grating Figure 13 shows the effect of noise on the ability of the method to detect strain induced changes in the spatial frequency of the grating. This figure shows the measured strain as computed from the spectral response of the grating when the Signal to Noise Ratio (SNR) is 200. The strain is a gaussian strain field with a standard deviation of 70mm, and a maximum strain of 25ppm. A 1m grating was simulated. The simulated grating was interogated over -30ppm to +30ppm at 1300nm, and 256 points were read. The results show significant tolerance for noise, and imply that noise will not be a limiting factor. In fact, the tuning range and speed of the laser are the limiting factor for the system.

Examination of the data shows that the stationary phase approximation does introduce error, particularly toward the far end of the grating. These errors do not preclude the use of this method as a distributed strain sensor, or as a method of evaluating the writing technique used to produce the grating. Grating reflectivities of as high as 16% are shown to introduce only minor distortions in $\tilde{K}(k)$.

V. Experiment and System Design

The previous sections have described and computationally demonstrated a theoretical system. In this section, I will add important details such as speed and resolution to the system. Specifications taken from the equipment to be used in the experiments will be presented. From these specifications, the expected performance of the system can be obtained. These numbers will provide a real world foundation with which experimental results could be evaluated. Two gratings will be considered: a high reflectivity (10%) 1cm grating, and a low reflectivity (0.1%) 1m grating.

Once the basic tolerances of the system have been described, a method of performing the vector measurement of the optical reflection spectrum will be described. The absence of any optical analog of the vector network analyzer is a bit disconcerting. It seems that either the field of coherent spectrum analyses has been neglected, or the construction of such a system is currently not feasible. Thermal analysis will show that although it will be necessary to use a great deal of care when constructing the fiber optic system, it should be possible to perform the measurements described above.

System Resolution, Spatial and Strain

The simple fourier transform relationship between the grating and the reflection spectrum of the grating makes the calculation of the system resolution relatively straight forward. I will assume white noise. Under this assumption the Signal-to-Noise-Ratio (SNR) of the spectrum, and the transformed grating are approximately equal. This computation can become a rather complicated problem if I allow the bandwidth to encompass many

wavelengths where there is little or no signal. To make the problem tractable, I will assume that the bandwidth is chosen intelligently, and that the above assumption holds as a rough approximation.

The strain resolution of the system is a function of the spatial resolution, d, the wavelength of light in the fiber, λ_f, and the SNR, S. The phase change over a single spatial element is given by,

$$\Theta_\varepsilon = \frac{4\pi d\varepsilon}{\lambda_f}, \tag{48}$$

where ε is the strain. The smallest resolvable phase change is given by

$$\Theta_{res} = \frac{1}{S}. \tag{49}$$

The minimum resolvable strain is then,

$$\varepsilon_{\min} = \frac{\lambda_f}{4\pi dS}. \tag{50}$$

The formula for the spatial resolution of the system is the same as the coherence length. An additional factor of two appears in the denominator because of the two appearing in the transform in equation (33).

$$d = \frac{\lambda^2}{\Delta\lambda} \cdot \frac{1}{2n}, \tag{51}$$

where n is the index of refraction of the fiber, and $\Delta\lambda$ is the range over which the laser can be tuned. The maximum length of an interrogated grating, L_g, is determined by the uncertainty or the

line width of the laser. given the line width in meters, $\delta\lambda$, the computation is the same, and

$$L_g = \frac{\lambda^2}{\delta\lambda} \cdot \frac{1}{2n} . \tag{52}$$

If the line width is given in hertz, $\delta\upsilon$,

$$L_g = \frac{c}{\delta\upsilon} \cdot \frac{1}{2n}, \tag{53}$$

where c is the speed of light in a vacuum.

Signal to Noise Ratio

The Signal to Noise Ratio (SNR), denoted by S above is determined by the reflectance of the grating, the power of the laser, the bandwidth of the system, and the Noise Equivalent Power (NEP, given in optical power per square root hertz) of the detectors. The NEP will be denoted by N_{EP}.

$$S = \frac{PR}{4N_{EP}\sqrt{BW}} \tag{54}$$

where P is the power of the laser, R is the reflectance of the grating, and BW is the system bandwidth. An additional factor of 4 is included in the denominator to account for coupler losses.

The bandwidth of the system is determined by the number of points that must be measured, N, and the time in which they must be measured, T. I will assume a settling time of two time constants, and that two measurements (real and imaginary) must be made for each point. The required bandwidth is then

$$BW = \frac{4N}{T}. \tag{55}$$

The final SNR is given by,

$$S = \frac{PR}{8N_{EP}\sqrt{\frac{N}{T}}}. \tag{56}$$

Thermal Considerations

As with most optical systems, thermal effects will be the predominant source of error. The optical thermal coefficient ρ, is about 8.8 ppm per degree Celsius [14]. The expected thermal drift given as degrees Celsius per second will be denoted by Φ, and the length of unmatched fiber will be denoted as L. The thermal drift in radians for a measurement is then

$$\Theta_T = 4\pi T \frac{L\Phi\rho}{\lambda_f}. \tag{57}$$

In an optimized system, the thermal phase error should be roughly equal to the noise induced phase error.

$$\Theta_{res} = \Theta_T. \tag{58}$$

$$\frac{8N_{EP}\sqrt{\frac{N}{T}}}{PR} = 4\pi T \frac{L\Phi\rho}{\lambda_f}. \tag{59}$$

Solving for T,

$$T = \sqrt[3]{N\left(\frac{2N_{EP}\lambda_f}{PR\pi L\Phi\rho}\right)^2}. \qquad (60)$$

Substituting into (56) to find S,

$$S = \frac{1}{8}\sqrt[3]{\frac{2\lambda_f P^2 R^2}{N_{EP}^2 N\pi L\Phi\rho}}. \qquad (61)$$

The scan rate and SNR are thus dictated by the thermal drift, the number of points to be measured, the power of the laser, and the noise produced by the detectors.

Evaluation of Experimental Systems

The experimental system is shown in Figure 20. The laser is split asymmetrically at the first coupler to use the light more efficiently and to cause the two beams of light at the interferometer to have a smaller difference in intensities. The laser is a 1mW tunable 1300nm laser diode system. There are two modes of tuning. One mode uses stepper motor tuning over 40nm in 0.1nm increments, and the other mode uses piezoelectric tuning over 0.33nm in a continuous sweep. The coarse tuning mode will be used for the 1cm sensor, and the fine tuning mode will be used for the 1m sensor. The instability of the laser over 50ms is 100kHz. The detectors used will be matched detectors with a Noise Equivalent Power of 11pW per square root Hz.

The parameters for the 1cm grating measurement system are shown below.

$\lambda_f = 890\times10^{-9}\,\mathrm{m}$	$P = 1\times10^{-3}\,\mathrm{w}$	$R = 0.1$
$N_{EP} = 11\times10^{-12}\,\mathrm{w}$	$N = 200\,\mathrm{pts}$	$L = 1.0\,\mathrm{m}$

$\Phi = .01\,{}^{\circ}\mathrm{C}/\mathrm{s}$ $\qquad \rho = 8.8\times10^{-6}\,\frac{1}{\mathrm{C}}\,\frac{\mathrm{rad}}{\mathrm{rad}}$ $\qquad \Delta\lambda = 40.0\,\mathrm{nm}$

Using these numbers in Eqn. (60), the optimum acquisition time, T, is found to be 464 microseconds. The laser would be unable to tune over the 40 nm band that quickly, so a more reasonable time of 20 milliseconds is assumed. This assumption results in an effective SNR, S, of 40 due to thermal instability. Computing the spatial and strain resolutions we find,

$$d = 14.4\times10^{-6}\,\mathrm{m}$$

$$\varepsilon_{\min} = 61\times10^{-6}\,\frac{\mathrm{m}}{\mathrm{m}}.$$

The parameters for the 1m measurement system are shown below.

$\lambda_f = 890\times10^{-9}\,\mathrm{m}$	$P = 1\times10^{-3}\,\mathrm{w}$	$R = 0.001$
$N_{EP} = 11\times10^{-12}\,\mathrm{w}$	$N = 100\,\mathrm{pts}$	$L = 1.0\,\mathrm{m}$
$\Phi = .01\,{}^{\circ}\mathrm{C}/\mathrm{s}$	$\rho = 8.8\times10^{-6}\,\frac{1}{\mathrm{C}}\,\frac{\mathrm{rad}}{\mathrm{rad}}$	$\Delta\lambda = 0.33\,\mathrm{nm}$

Using these numbers in Eqn. (60), the optimum acquisistion time, T, is found to be 8ms. The SNR under these conditions is 100. Computing the spatial and strain resolutions we find,

$$d = 1.7\times10^{-3}\,\mathrm{m}$$

$$\varepsilon_{\min} = 0.2\times10^{-6}\,\frac{\mathrm{m}}{\mathrm{m}}.$$

The spatial and strain resolutions over 1m are compatible with large structures under small loads. The limiting factor for this system is the expected low reflectivity of long gratings. It is not unreasonable to expect that higher reflectances can be obtained in the near term (3-5 years). The spatial and strain resolutions over a 1cm grating allow for the detection of only very

large strains. In the case of crack detection the strain sensitivity may be sufficient in cases where spatial resolution is more important than strain resolution. The limiting technology for the 1 cm grating is the speed with which the laser can tune over large wavelengths.

Vector Measurement System

Figure 20 shows the anticipated experimental set-up. The coupler following the laser is unbalanced because the reflectivity of the grating is expected to be small. More light is budgeted for the measurement leg for this reason. The system is optimised for a 10% reflection. The symetric layout of the system will allow bundling of the fibers in corresponding sections of the reference and measurement leg. This bundling will reduce some of the thermal drift.

The primary concern with this design is polarization control. None has been built into the system, and it could be a severe problem. If later calculations or experiments show that such control is needed, then polarization maintaining fiber and couplers may be needed throughout. This requirement would significantly raise the cost of the system.

Experimental Procedure

The first measurement that will be attempted will be to determine the amplitude of the modulation of the index of refraction forming a Bragg grating. This measurement can be divided into three steps. The first is the determination of the experimental parameters such as the total wavelength change to be swept, the step change in the wavelength over the sweep, and the expected range of the power of the reflected light. The second step is the calibration of the system at the experimental

parameters discussed above. The final step is the actual measurement of the Bragg grating.

The optimal wavelength sweep and step size are determined by the length of the grating to be measured. The grating length is expected to be known to within 20%. The measurement range will be chosen to be twice the expected grating length giving a required wavelength uncertainty from Eqn. (52) of

$$\delta\lambda = \frac{\lambda^2}{nL_g}. \qquad (62)$$

The sweep range is chosen such that there will be N samples over the length and is given as,

$$\Delta\lambda = \frac{N\lambda^2}{2L_g n}. \qquad (63)$$

The reflectance of the grating will be a more difficult parameter to know prior to the conducting of the experiment. Measurement with a broadband source and a spectrum analyzer will not produce an accurate measurement due to the narrow linewidths produced by Bragg gratings. Estimations based upon exposure time and incident power will need to be used to get an order of magnitude response. Even then, the poorly understood nature of the reaction involved will probably lead to significant errors. As a result, the gain on the receiver will probably need to be adjusted during the measurement phase of the experiment.

Calibration of the system will be necessary to remove the effects of intensity changes of the laser output as a function of the wavelength. The wavelength as a function of tuning voltage (or current) will also need to be calibrated. In addition, calibration on a known source will provide good measurements of systematic thermal drift and noise levels.

Calibration of the laser will be accomplished by replacing the Bragg grating in Figure 20 with a cleaved fiber. The cleaved fiber will produce a 3.5% reflection. Sweeping the laser over its tuning range, and measuring the interference fringes will produce a calibration of both the linearity of the wavelength sweep, and the output power of the laser as a function of wavelength. The exact wavelength versus controlling parameter relationship can be obtained if the difference in the reference and measurement pathlengths is known, or if it is changed by a known amount. A known change can be introduced by adding a section of fiber onto the measurement length with a splice tube, and index matching gel.

All of the calibration steps shown above can be achieved without the use of the PZT modulator. The modulator can be calibrated by holding the laser wavelength constant, and sweeping the PZT control voltage through its entire range. The resulting interference measurement can be used to determine the appropriate control voltages to achieve the required quadrature phase shift.

Once the system has been calibrated, the measurement of the Bragg grating can proceed. The real and imaginary (in-phase and quadrature) components of the reflection spectrum of the grating will be measured at each previously defined wavelength. The resulting spectral measurements will then be normalized to 100% based upon the 3.5% calibration measurements. The wavelength for each point will be converted its corresponding intrafiber-wavenumber. The complex reflectance as a function of wavenumber will then be entered into the FORTRAN code in the Appendix. A profile of the complex modulation of the Bragg grating will then be produced.

This profile will decribe the amplitude of the index of refraction modulation, as well as the phase of the index of refraction modulation. The quantitiy computed will be a complex $\frac{\Delta n(z)}{n}$. Computing the phase difference between adjacent sections of the grating will produce a measurement of the local freqency of of the index of refraction modulation. This frequency is directly related to the local strain in the fiber. As with all intrinsic sensors, this strain measurement will contain poisson cross terms from shear and compressional strain as well as temperature and axial strain components.

The spatial frequency of $\frac{\Delta n(z)}{n}$ must remain within the range of the interrogating tunable laser. Other than this requirement and the requirement that the total reflection at a given wavelength remain small, no other conditions are placed on $\frac{\Delta n(z)}{n}$. If the spatial frequency of $\frac{\Delta n(z)}{n}$ is outside of the lasers tuning range at any z, the system fails gracefully, and the amplitude of $\frac{\Delta n(z)}{n}$ is measured to be zero at z .

VI. Creation of Long Bragg Gratings

The work described in Section V demonstrates that it should be possible to determine the strain in a Bragg grating as a function of length along a fiber core. The work also demonstrates that using existing tunable lasers, Bragg gratings 1 m long could be interrogated for small strains with a resolution on the order of 1mm. However the problem of obtaining such a 1m grating is not trivial. Current methods such as phase masks and holographic techniques generally write gratings that are no more than 1cm long. In addition, the need to strip the buffer off of the fiber before writing these gratings will embrittle the fiber.

The Hill method of writing gratings can easily write a grating over 1m of fiber. Unfortunately, the grating is at the frequency of the writing laser, and cannot be interrogated by a laser at a different frequency. Hill originally wrote gratings with a 488nm laser. It was later discovered that this was a two photon process. Holographic and phasemask methods have much lower power densities, and must use laser light around 244nm. This movement to a single photon reaction results in an increase in efficiency by a factor of about 1 million. If we were to attempt use a 3 photon process to write a grating with a 1300nm laser we would expect to encounter a similar loss in efficiency. This attempt would result in writing times on the order of 7 years.

The Hill method is appealing, however, because it does not involve the removal of the buffer coating, and requires no bulk optics other than a means of coupling the laser light into a single mode fiber. In order to use the Hill method to write gratings at 1300nm, we will rely upon the nonlinear nature of the index of refraction change.

We will assume that the process is not reversable, and that the probability of an absorption center changing states is proportionally related to the local intensity of light by some quantum efficiency, $Q(\lambda)$. From these assumptions, we get a simple expression for the change in index of refraction as a result exposure to a given amount of energy,

$$\Delta\varepsilon = \Delta\varepsilon_{sat}\left(1 - e^{-Q(\lambda)\Lambda t}\right). \tag{64}$$

where Λ is the power flux given in watts per meter squared, and where t is the time of exposure. $Q(\lambda)$ is the quantum efficiency of the process given in meters squared per joule.

Since this process becomes nonlinear for large values of Λt, if two different standing waves are set up in the fiber, the sum and difference frequencies will be produced. Figures 14 through 17 demonstrates how this lower frequency grating is produced. In figures 14 through 17, the maximum incident energy density for each standing wave, and a uniform exposure field is assumed to be equal to the the inverse of the quantum efficiency. This produces significant harmonics.

In general, we cannot produce an arbitrarily high exposure in the fiber when using the Hill technique for writing gratings. The limiting factor becomes the penetration of the light into the grating. As the grating is written, it reflects more of the incident light, and at 100% reflection, the far end of the grating is no longer being exposed. Continued exposure lengthens the grating but does not increase the amplitude of the index of refraction modulation. A rough approximation of the modulation of the index of refraction at 100% reflection can be obtained from the equation for the coupling coefficient in Eqn. (44).

$$C = \frac{\beta m N \Delta x}{2} = \frac{\pi L m}{\lambda_f} . \tag{65}$$

Assuming that 100% reflection occurs when C = 1,

$$m = \frac{\lambda_f}{\pi L}. \tag{66}$$

In this case, L is one half of the coherence length of the laser, and denotes the approximate length of the standing wave pattern in the fiber. The relative change in the index of refraction is given by m.

Given the maximum standing wave modulation, the only parameter available for control is the uniform bias exposure. The computation of the optimum bias level for harmonic generation does not lend itself to analytic methods. Therefore computational methods were employed to generate the plots shown in Figures 18 and 19. Figure 18 is a plot of the optimum bias level as a function of the modulation depth. Both axis have been normalized to the quantum efficiency. Figure 19 is a plot of the magnitude of the difference frequency generated from the nonlinear effects and the modulation frequencies. The magnitude of the difference frequency is given relative to the modulation frequency, and the modulation depth has gain been normalized to the quantum efficiency. Since the modulation gratings have 100% reflectivities, the y axis also gives the reflectivity of the difference frequency grating at the first order resonance frequency.

Quantitative values for much of the above work can be obtained from a 1993 paper by D. L. Williams et al.[7] First, $\mathcal{Q}(\lambda)$, can be determined from the power flux and exposure time to saturation given in the paper. From this I find that,

$$Q(244\text{nm}) = 3\times10^{-9}\,\frac{\text{m}^2}{\text{J}}$$

At 488nm, we assume that the quantum efficiency decreases by a factor of one million.

$$Q(488\text{nm}) = 3\times10^{-15}\,\frac{\text{m}^2}{\text{J}}.$$

For a one meter grating, the maximum modulation depth, m, at 488nm,

$$m = 100\times10^{-9}.$$

D.L. Williams et al.[7] give a saturated index of refraction value of 34 ppm for standard germanium doped communications fiber. In order to produce the above value of modulation depth, the energy flux normalized to the quantum efficiency would be .0044. looking on Figure 19, we find that the maximum generated difference frequency amplitude would be below 1ppm. We can conclude from this that standard germanium doped communications fiber will not produce difference frequency gratings. A fiber with a saturated index of refraction change around 0.1 ppm is needed, and this corresponds to a doping level of about 0.02mol% germanium.

Such a fiber could be created by doping the glass uniformly at 0.02% mol germanium, and then doping the cladding with a dopant that lowers the index of refraction of the glass. Fluoride is a commonly used index lowering dopant. Boron would not be a good choice as a cladding dopant because it appears to enhance the photoinduced index of refraction change.

VII Conclusion

This thesis has presented most of the analysis necessary to contruct a distributed fiber-optic strain and/or temperature sensing system. The analysis can be divided into three general sections: the basic theory behind the technique; effects of error sources and real world restrictions on measurements; and construction of the sensor. A detailed analysis of the means of making the vector measurement has not been performed, and polarization effects in particular have not been addressed.

A method of measuring the slow spatial variation of a Bragg grating in both phase and amplitude has been computationally demonstrated, and shown to be feasible. This method would permit the development of distributed fiber-optic strain sensors. This method would also be useful as tool in the writing and evaluation of Bragg gratings.

Analysis of the system specifications shows that this method of measuring strain could provide significant advantages over all current methods of strain measurement. In cases where the variation of strain along a line must be measured and many strain guages would be required, this system could offer a cost savings due to the simplicity of the sensor, and the increased sensitivity of the sensor.

A method of writing long Bragg gratings at telecommunications wavelengths has been described. This method uses the non-linear nature of the index of refraction change to produce the long gratings using standing waves around 488nm. Calculations show that custom fibers with low germanium concentrations in the core will be necessary to produce these long gratings.

Although foil guages and their associated hardware are relatively cheap, the bulk of the cost of using them lies in the attachment and wiring of each individual strain guage. In applications where hundreds of strain guages are needed, The attachment of a single fiber could be achieved in minutes or hours instead of the weeks that would likely be needed to attach and wire hundreds of individual foil strain guages.

If the cost per channel for foil guages is $200, and the cost for the fiber-optic system described here is $50000, the break even point occurs a 250 channels. If we then consider the cost of attaching and wiring 250 foil guages, at 10 minutes per guage, and $12 per hour, this comes to $500. Thus if a single fiber sensor could be bought and attached for $500, and 250 discrete measurements of strain along a line were desired, the system would be cost effective.

Of course any significantly different system such as this one is likely to find applications where the foil strain guages simply would not work. Use in electromagnetically noisy environments and for submillimeter strain resolutions are example applications where strain guages are ineffective.

A full developement of this technique could provide a new and very valuable tool for the measurement of strain and temperature in both embedded health monitoring, and externally attached strain measurement. The measurement method could also be applied to any phenomenon that causes a small change in the index of refraction of the fiber core.

Appendix-FORTRAN Code

```
      PROGRAM BRAGCOEF
      COMPLEX*16 D(16384),REFLECTION
      REAL*16 DEPSILON,BETA,PI,PPM,ZETA,DZ,LENGTH
      REAL*16 MAXZETA,COUP
      INTEGER N,ASIZE,J
CHARACTER*256 OUTNAME,INNAME

       PI = 3.14159
       BETA = 2.0*PI/(.6*1300E-9)

 WRITE(*,*) 'ENTER OUTPUT FILENAME WITH QUOTES'
 READ(*,*) OUTNAME

 WRITE(*,*) 'ENTER INPUT FILENAME WITH QUOTES'
 READ(*,*) INNAME

 WRITE(*,*) 'ENTER MAXIMUM WAVELENGTH DEVIATION (PPM)'
 READ(*,*) PPM
       MAXZETA = BETA*PPM*1E-6

 WRITE(*,*) 'ENTER MAXIMUM COUPLING FACTOR'
 READ(*,*) COUP

 OPEN(12,FILE=OUTNAME,STATUS = 'NEW')
       OPEN(9,FILE=INNAME,STATUS='OLD')

       READ(9,*)ASIZE
       READ(9,*) LENGTH

       DZ = LENGTH/REAL(ASIZE)
       DEPSILON = 2.0*COUP/(BETA*LENGTH)
       WRITE(*,*) 'MODULATION DEPTH IS',DEPSILON

       DO N = 1, ASIZE
```

```
            READ(9,*) D(N)
         ENDDO

        DO J = -127,127
            ZETA = REAL(J)*MAXZETA/127
        CALL COEF(ZETA,REFLECTION,D,ASIZE,DEPSILON,DZ,BETA)
            RCA = ABS(REFLECTION)*ABS(REFLECTION)
            WRITE(*,*)ZETA,RCA
            WRITE(12,100)ZETA,REFLECTION
100      FORMAT(F9.1,',',F12.10,',',F12.10)
        ENDDO
        STOP
        END


        SUBROUTINE
COEF(ZETA,REFLECTION,D,ASIZE,DEPSILON,DZ,BETA)
        COMPLEX*16 D(16384),FORWARD(16384),EXPO
        COMPLEX*16 BACKWARD(16384),CK(16384),REFLECTION
        REAL*16 ZETA,DZ,DEPSILON,BETA
        INTEGER N,ASIZE,J

         DO N = 1, ASIZE
            EXPO = EXP( (0.0,-1.0)*2.0*ZETA*REAL(N)*DZ)
            CK(N) = EXPO*BETA*DZ*(0.0,-0.5)*DEPSILON
            FORWARD(N) = (1.0,0.0)
            BACKWARD(N) = (0.0,0.0)
        ENDDO

        DO J = 1,15
            CALL REFLECT(D,FORWARD,BACKWARD,CK,ASIZE)
            CALL TRANSMIT(D,FORWARD,BACKWARD,CK,ASIZE)
        ENDDO
        REFLECTION = BACKWARD(1)
```

```
      RETURN
      END


      SUBROUTINE REFLECT(D,FORWARD,BACKWARD,CK,ASIZE)
      COMPLEX*16
REFLECTION,D(16384),CK(16384),FORWARD(16384)
      COMPLEX*16 BACKWARD(16384),PROD
      INTEGER ASIZE,N

      BACKWARD(ASIZE) = D(ASIZE)*FORWARD(ASIZE)*CK(ASIZE)
      DO N = ASIZE-1,1,-1
            PROD = D(N)*FORWARD(N)*CK(N)
            BACKWARD(N) = BACKWARD(N+1) + PROD
       ENDDO
       RETURN
       END


      SUBROUTINE TRANSMIT(D,FORWARD,BACKWARD,CK,ASIZE)
      COMPLEX*16
REFLECTION,D(16384),CK(16384),FORWARD(16384)
      COMPLEX*16 BACKWARD(16384),PROD
      INTEGER ASIZE,N

       FORWARD(1) = CONJG(D(1))*BACKWARD(1)*CONJG(CK(1)) +1
      DO N = 2, ASIZE
            PROD =CONJG(D(N))*BACKWARD(N)*CONJG(CK(N))
            FORWARD(N) = FORWARD(N-1) + PROD
       ENDDO
       RETURN
       END
```

```
      PROGRAM FINDGRAT
      COMPLEX*16
D(1024),REFL(1024),CK(1024),G(1024),ZCOM
      COMPLEX*16 MAG(1024),ANG(1024),G0,IMD
      REAL*16 BETA,PI,ZETA,DZ,DA,GA,WKN
      REAL*16 MAXZETA,ZREAL,ZIMAG,DANG
      INTEGER N,ASIZE,J,K,K0
      CHARACTER*256 OUTNAME,INNAME

       PI = 3.14159
       BETA = 2*PI/(.6*1300E-9)

    WRITE(*,*) 'ENTER OUTPUT FILENAME WITH QUOTES'
    READ(*,*) OUTNAME

    WRITE(*,*) 'ENTER INPUT FILENAME WITH QUOTES'
    READ(*,*) INNAME

       OPEN(11,FILE=OUTNAME,STATUS = 'NEW')
       OPEN(9,FILE=INNAME,STATUS='OLD')
       ASIZE = 256
       K= 1
       J=1
       WRITE(*,*) 'ENTERING FILE READING LOOP'
       DO N = 1,ASIZE
             READ(9,200,END=100) ZETA,ZREAL,ZIMAG
200    FORMAT(F9.1,X,F12.10,X,F12.10)
             ZCOM = CMPLX(ZREAL,ZIMAG)
              REFL(N) = ZCOM
              IF (ZETA.EQ.0) THEN
                   G0 = ZCOM
                   K0 = N
               ENDIF
       ENDDO
```

```
100         WRITE(*,*)'EXITING FILE READING LOOP'
        DZ = REAL(N)*PI/ZETA/ASIZE/2.0
        WRITE(*,*) DZ
        WRITE(*,*) BETA
        CALL FFT(REFL,8)
        WRITE(*,*) 'RETURN FORM FFT'
        DO N = 1, ASIZE
            G(N) = REFL(ASIZE - N +1)
            CK(N) = BETA*DZ*(0.0,-0.5)
       ENDDO
      WRITE(*,*) 'STARTING ITERATIONS'

       DO N = 1,ASIZE
                     D(N) = G(N)*(0.0,2.0)/BETA/PI
       END DO
       WRITE(*,*) K0
       DO J = 1,ASIZE
             WKN = 2.0*PI*REAL(J)*REAL(K0)/REAL(ASIZE)
             D(J) = D(J)*EXP((0.0,-1.0)*WKN)
             MAG(J) = SQRT(REAL(CONJG(D(J))*D(J)))
             IMD = (0.0,-1.0)*D(J)
             ANG(J) = ATAN2(REAL(D(J)),REAL(IMD))
       ENDDO
       DO J = 1,ASIZE
           ZREAL = REAL(J)*DZ
           IF (J.EQ.1) THEN
                    DANG = 0.0
                    ELSE
                    DANG = ANG(J) - ANG(J-1)
                    IF (DANG.LT.-PI) DANG = DANG + 2*PI
                    IF (DANG.GT.PI) DANG = DANG -2*PI
           ENDIF
           DA = 39.5*ABS(D(J))*1E6
```

```
            DANG = 1E6*DANG/DZ/BETA
            WRITE(11,300)ZREAL, DA,DANG
300     FORMAT(F7.4,',',F10.5,',',F10.5)
        END DO


        STOP
        END


      SUBROUTINE FFT(X,NU)
      COMPLEX*16 X(32768),U,W,T
            INTEGER NU
      N = 2**NU
      PI= 3.141593
      DO 20 L = 1,NU
      LE = 2**(NU+1-L)
      LE1=LE/2
      U=(1.,0.)
      W=CMPLX(COS(PI/FLOAT(LE1)),-SIN(PI/FLOAT(LE1)))
          DO 20 J=1,LE1
          DO 10 I=J,N,LE
                    IP=I+LE1
                    T=X(I) +X(IP)
                    X(IP)=(X(I)-X(IP))*U
 10       X(I)=T
 20       U=U*W
      NV2=N/2
      NM1=N-1
      J=1
      DO 30 I=1,NM1
          IF (I.GE.J) GO TO 25
            T=X(J)
            X(J)=X(I)
```

```
            X(I) = T
25        K=NV2
26        IF (K.GE.J) GO TO 30
            J=J-K
            K=K/2
          GO TO 26
30    J=J+K
      RETURN
      END
```

References

[1] K. O. Hill, Y. Fujii, D. C. Johnson, and B. S. Kawasaki, "Photosensitivity in optical fiber waveguides: Application to reflection filter fabrication," Applied Physics Letters, May 1978, Vol. 32, No. 10, pp 647-649.

[2] D. K. W Lam and B. K. Garside, "Characterization of single-mode optical fiber filters," Applied Optics, Feb. 1981, Vol. 20, No. 3, pp 440-445.

[3] G. Meltz, W.W. Morey, and W. H. Glenn, "Formation of Bragg gratings in optical fibers by a transverse holographic method," Optics Letters, 1989, Vol. 14, No. 15, pp 823-825

[4] B. Malo, K. O. Hill, F. Bilodeau, D. C. Johnson, and J. Albert, "Point-by-Point Fabrication of Micro-Bragg Gratings in Photosensitive Fibre Using Single Excimer Pulse Refractive Index Modification Techniques," Electronics Letters, Sept. 1993, Vol. 29, No. 18, pp 1668-1669.

[5] K. O. Hill, B. Malo, F. Bilodeau, D. C. Johnson, and J. Albert, "Bragg gratings fabricated in monomode photosensitive optical fiber by UV exposure through a phase mask," Applied Physics Letters, March 1993, Vol. 62, No. 10, pp 1035-1037.

[6] R. M. Atkins, et al., "Enhanced Photo-induced refractive index changes in optical fibers via low temperature hydrogen loading," CLEO, Baltimore, Md. 1993, CPD 20.

[7] D. L. Williams, B. J. Ainslie, J. R. Armitage, R. Kashyap, and R. Campbell, "Enhanced UV Photosensitivity in Boron Codoped

Germanosilicate Fibres," Electronics Letters, Jan. 1993, Vol. 29, No. 1, pp 45-46.

[8] K. O. Hill, "Aperiodic Distributed-Parameter Waveguides for Integrated Optics," Applied Optics, Aug. 1974, Vol. 13, No. 8. pp 1853-1856.

[9] M. Matsuhara and K. O. Hill, "Optical-Waveguide Band-Rejection Filters: Design," Applied Optics, Dec. 1974, Vol. 13, No. 12, pp 2886-2888.

[10] J. P. Bernardin and N. M. Lawandy, "Dynamics of the formation of Bragg gratings in germanosilicate optical fibers," Optics Communications, Oct. 1990, Vol. 79, NO.. 3.4, pp194-199.

[11] S. M. Melle, A. T. Alavie, S. Karr, T. Coroy, K. Liu, and R. M. Measures, "A Bragg Grating-Tuned Fiber Laser Strain Sensor System," IEEE Photonics Technology Letters, Feb 1993, Vol. 5, No. 2, pp 263-266.

[12] G. A. Ball, W. W. Morey, and P. K. Cheo, "Single- and Multipoint Fiber-Laser Sensors," IEEE Photonics Technology Letters, Feb. 1993, Vol. 5, No. 2, pp 267-270.

[13] D. Bullock, J. Dunphy, and G. Hufstetler, "Embedded Bragg grating fiber optic sensor for composite flexbeams," Proceedings of SPIE, Fiber Optic Smart Structures and Skins V, 1992, Vol. 1798, pp 253-261.

[14] W. W. Morey, J. R. Dunphy, and G. Meltz, "Multiplexing fiber bragg grating sensors," Proceeding of SPIE, Distributed and Multiplexed Fiber Optic Sensors, 1991, Vol. 1586, pp 216-224.

[15] W. W. Morey, G. Meltz, and W. H. Glenn, "Fiber optic Bragg grating sensors," Proceedings of SPIE, Fiber Optic and Laser Sensors VII, 1989, Vol. 1169, pp 98-107.

[16] A. D. Kersey, T. A. Berkoff, and W. W. Morey, "High-resolution Fibre-Grating Based Strain Sensor with Interferometric Wavelength-Shift Detection," Electronics Letters, Jan 1992, Vol. 28, No. 3, pp 236-238.

Figures

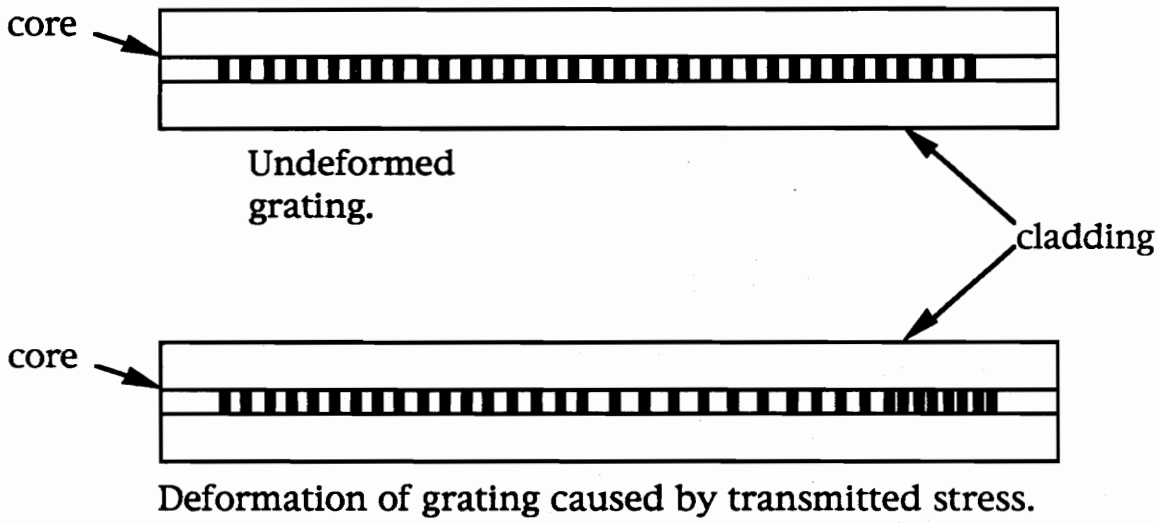

Figure 1. Example of Bragg grating distributed sensor before and after load is applied.

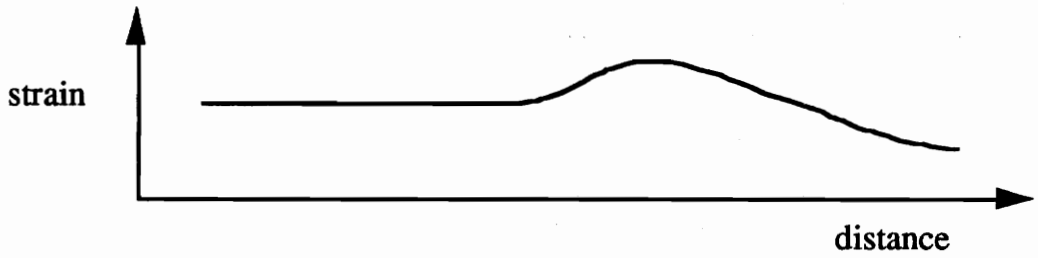

Figure 2. Example of how the deformation caused by the load in figure 1 would be displayed as strain.

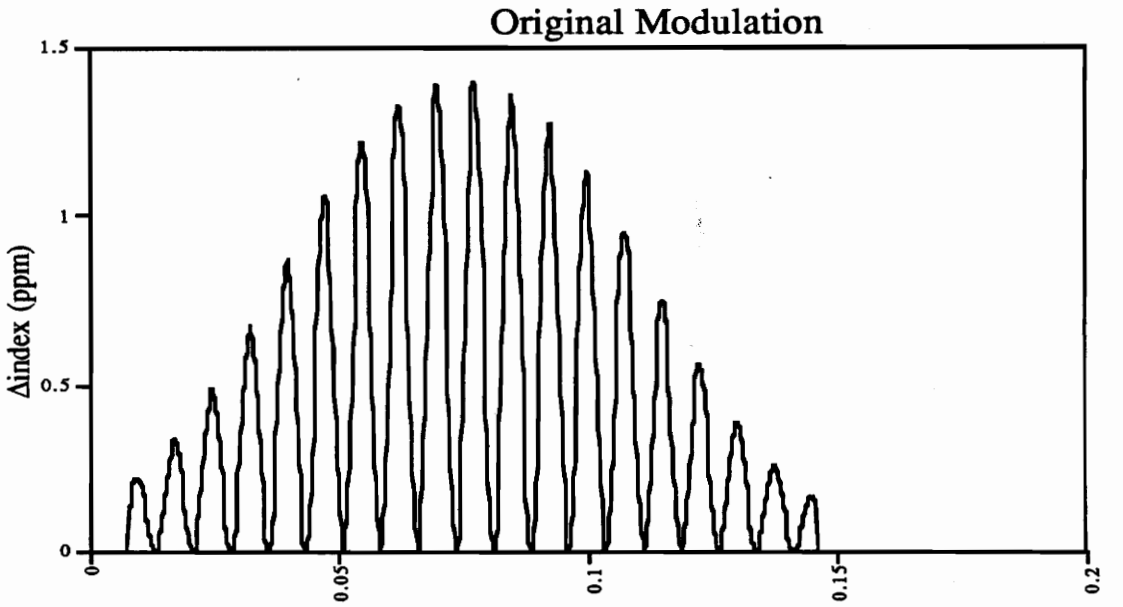

Figure 3. Amplitude profile of a gaussian Bragg grating modulated by a sine function.

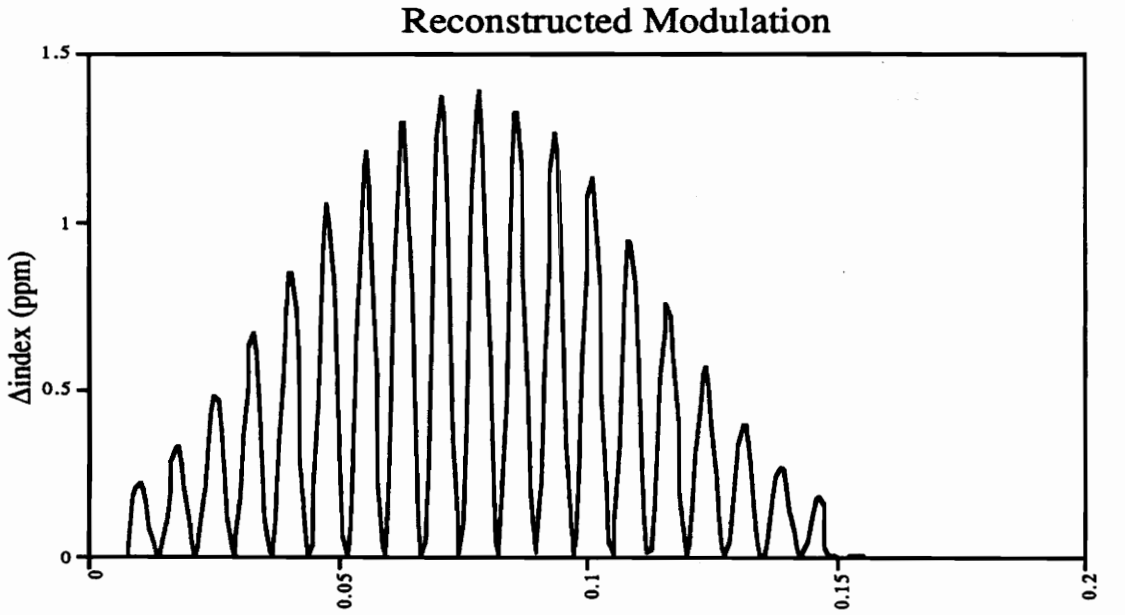

Figure 4. Scaled Fourier Transform of the reflection spectrum. Note the error in the form of an offset as the distance into the grating increases.

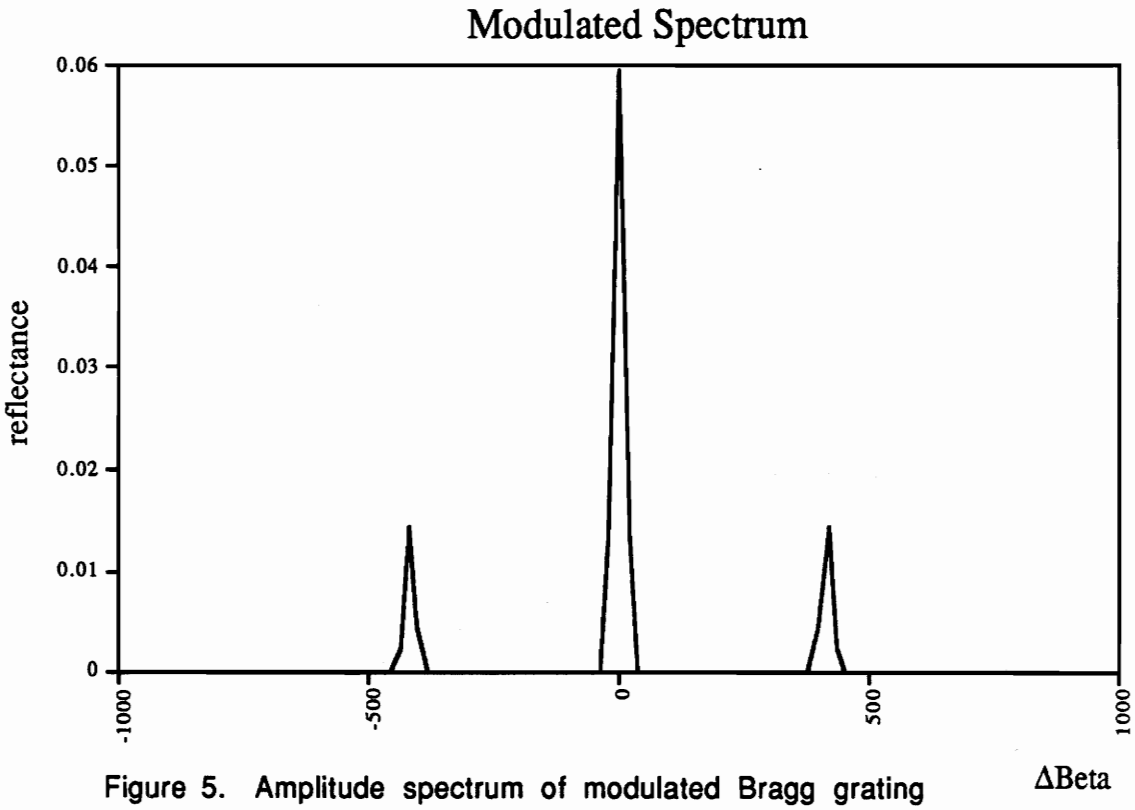

Figure 5. Amplitude spectrum of modulated Bragg grating shown in figure 3. Note the presence of sidebands as a fourier transform relationship would predict.

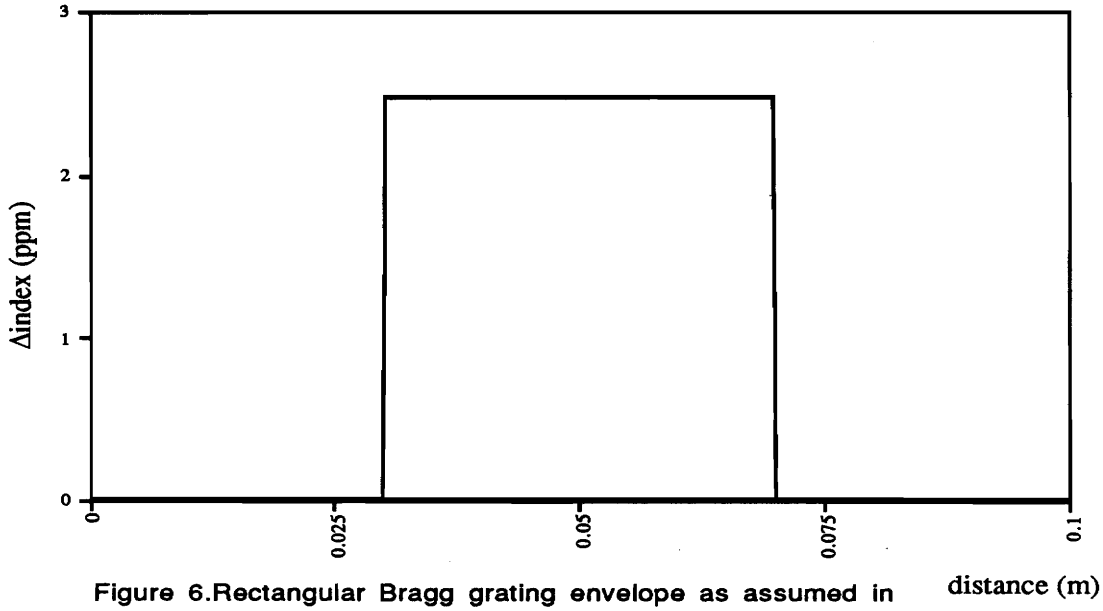

Figure 6.Rectangular Bragg grating envelope as assumed in many published models.

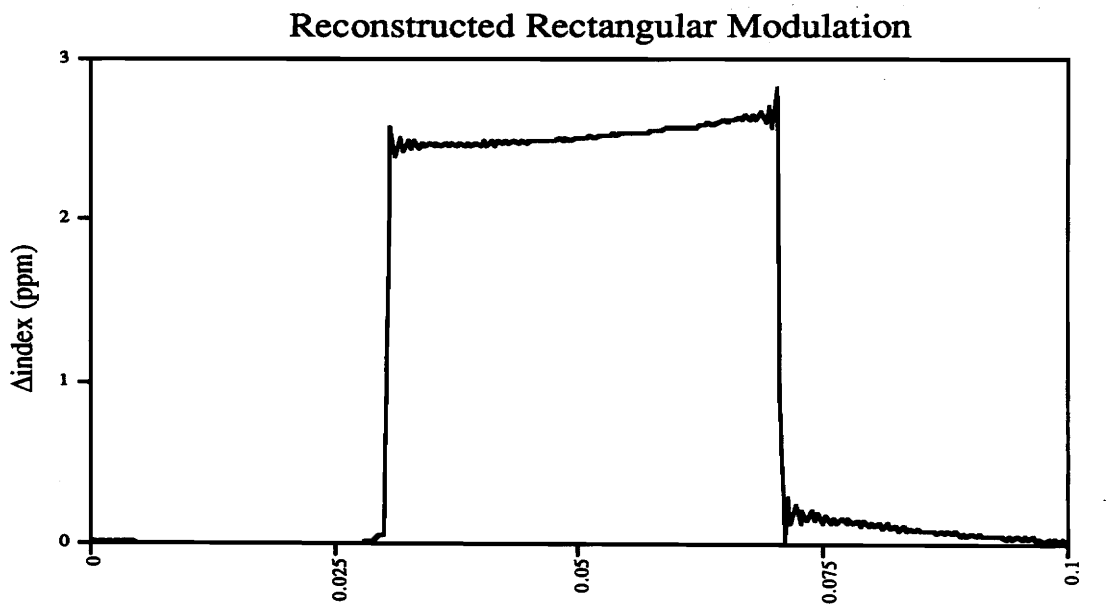

Figure 7. Reconstructed rectangular modulation with characteristic oscillations at discontinuities.

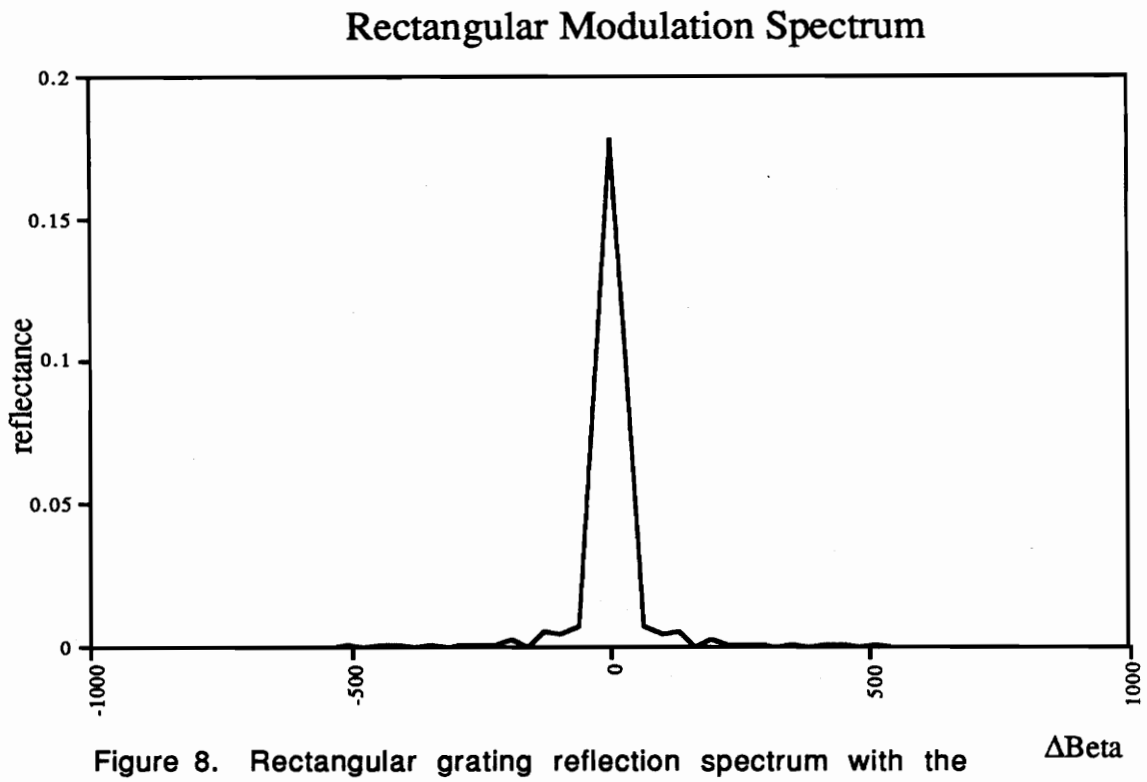

Figure 8. Rectangular grating reflection spectrum with the expected Sync structure.

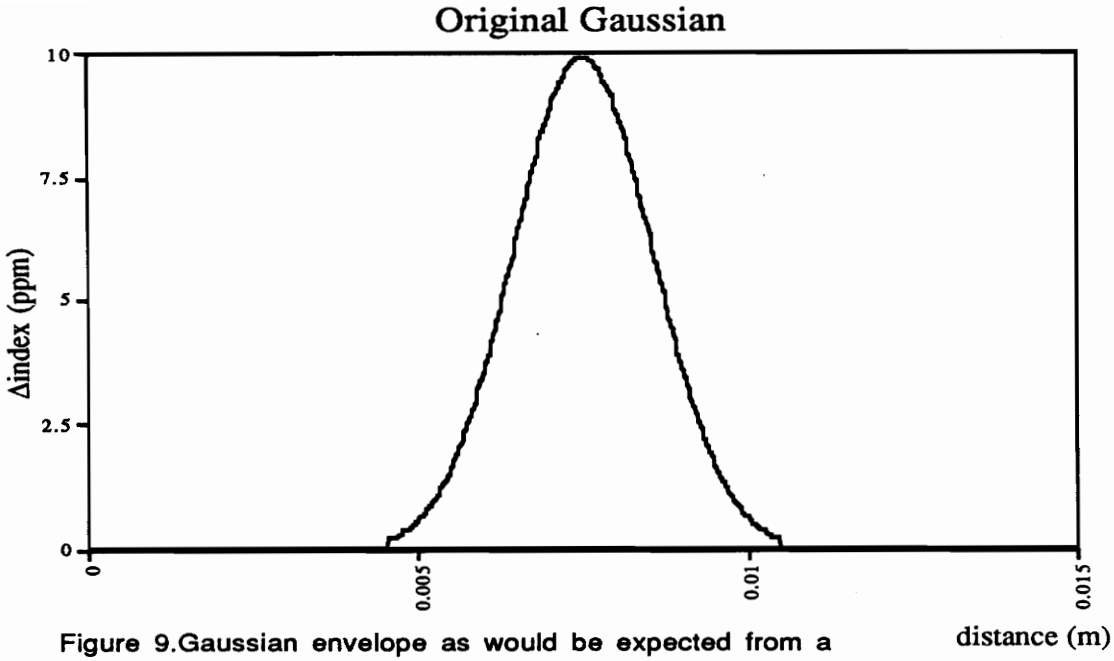

Figure 9.Gaussian envelope as would be expected from a grating formed by a single mode laser.

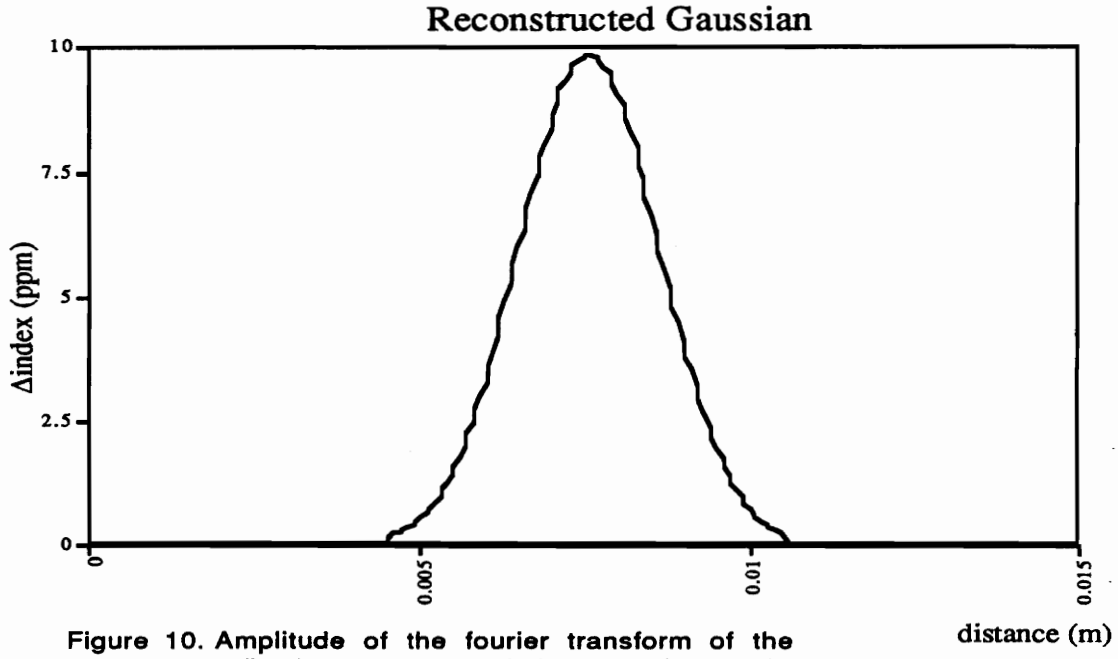

Figure 10. Amplitude of the fourier transform of the reflection spectrum of the gaussian envleope.

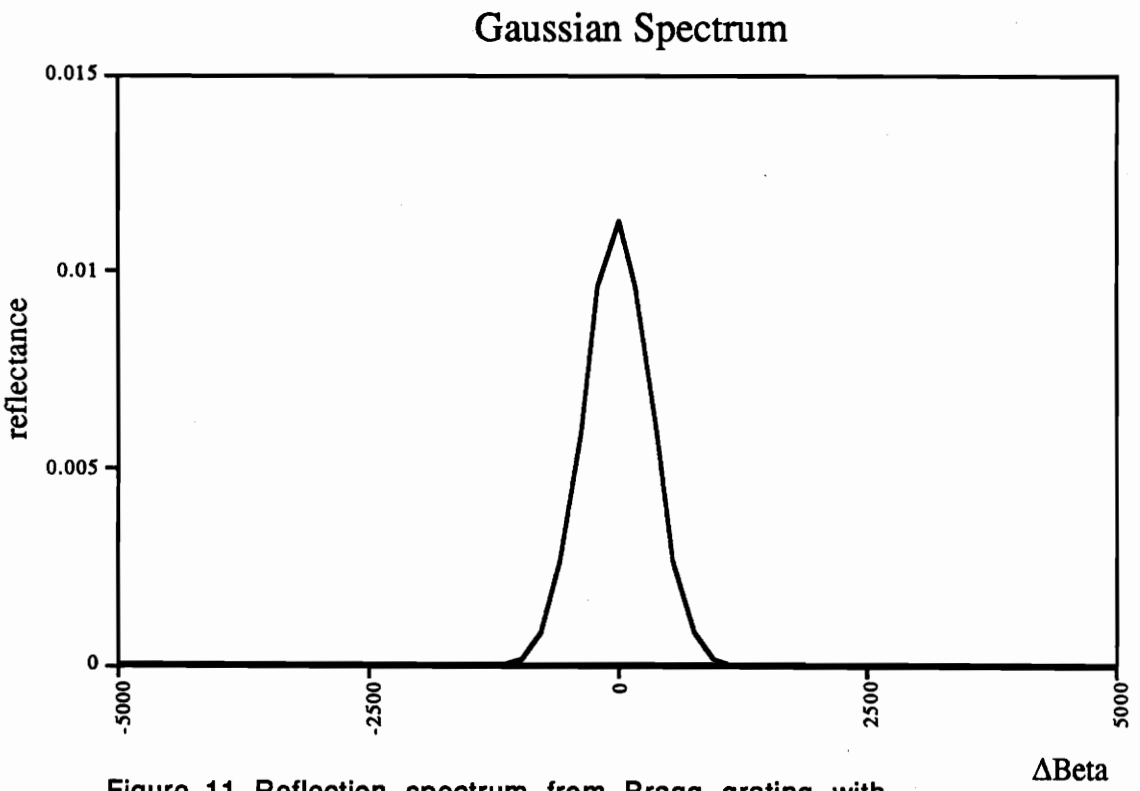

Figure 11. Reflection spectrum from Bragg grating with gaussian envelope.

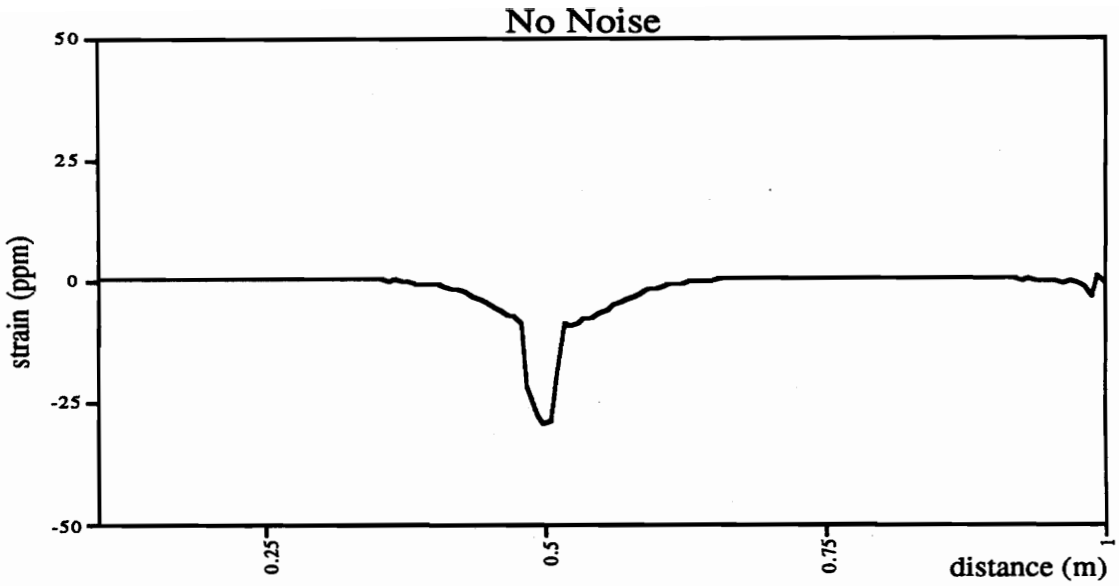

Figure 12. Strain as a function of distance along the core of a fiber computed from the reflected spectrum in the absence of noise.

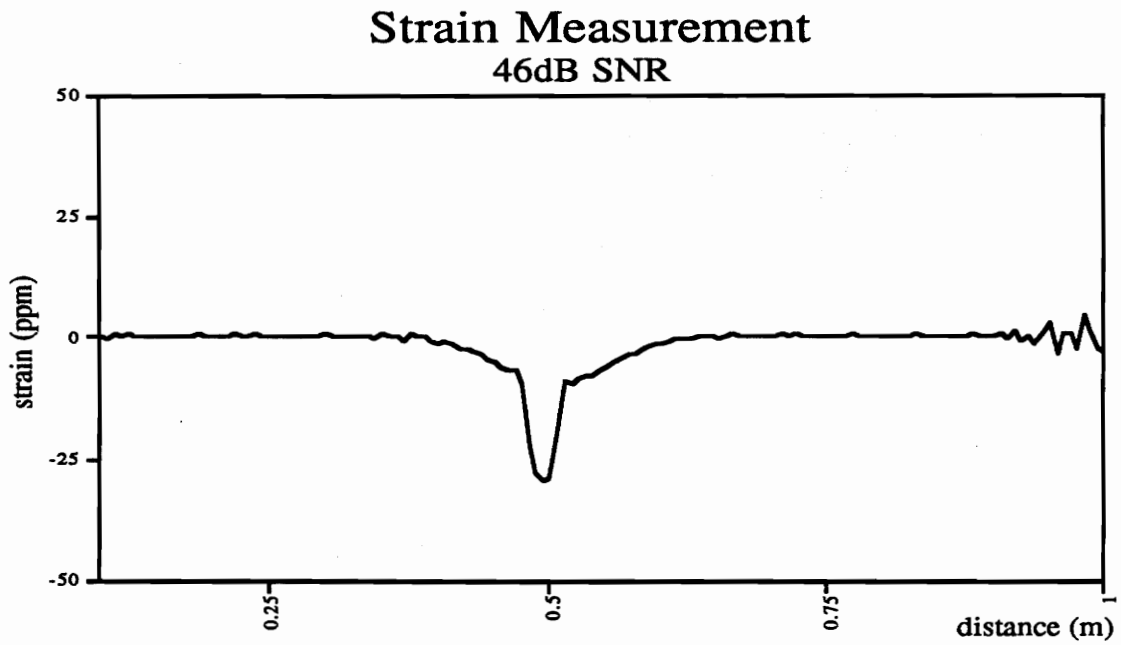

Figure 13. Strain along the core of a fiber computed from the reflected spectrum in the presence of noise.

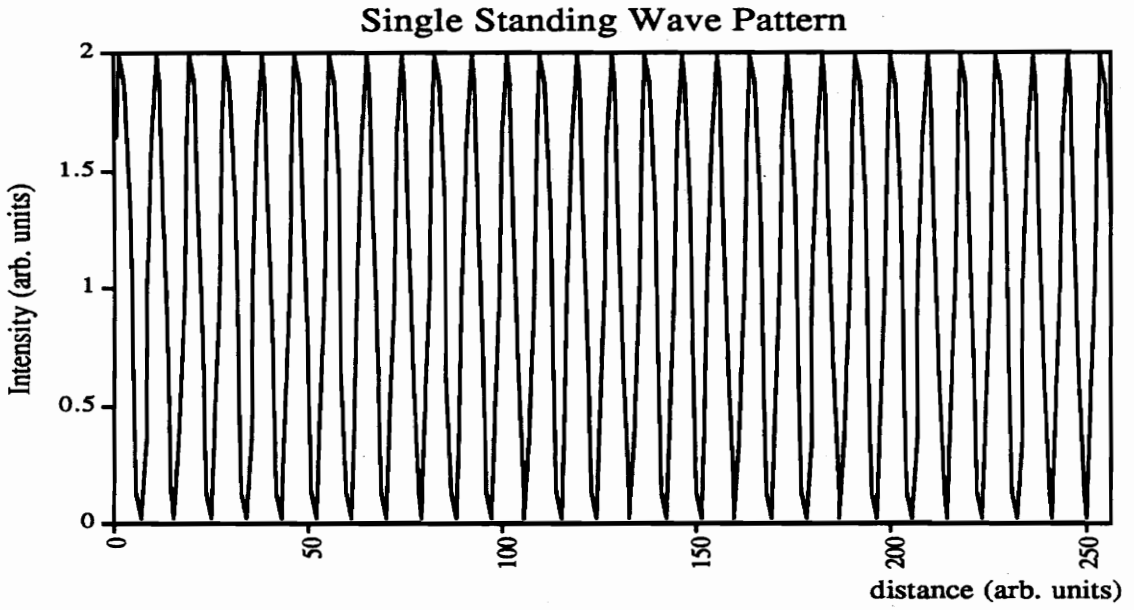

Figure 14. Standing wave pattern representing the illumination of the core of an optical fiber when using the Hill method of writing gratings.

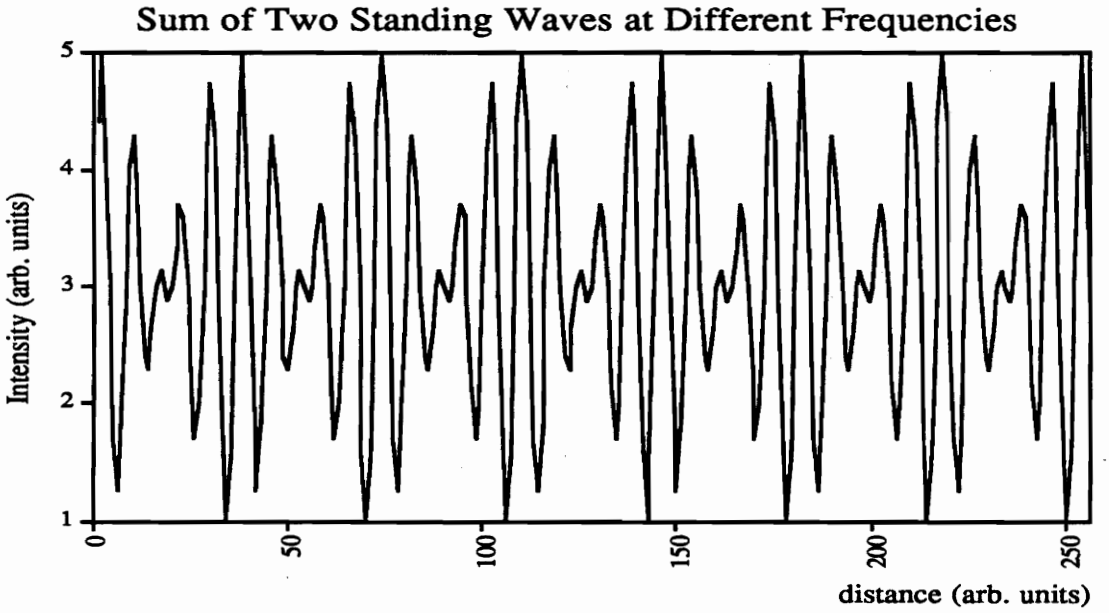

Figure 15. Standing wave pattern resulting when two wavelengths of light are coupled into an optical fiber with a reflector at the other end.

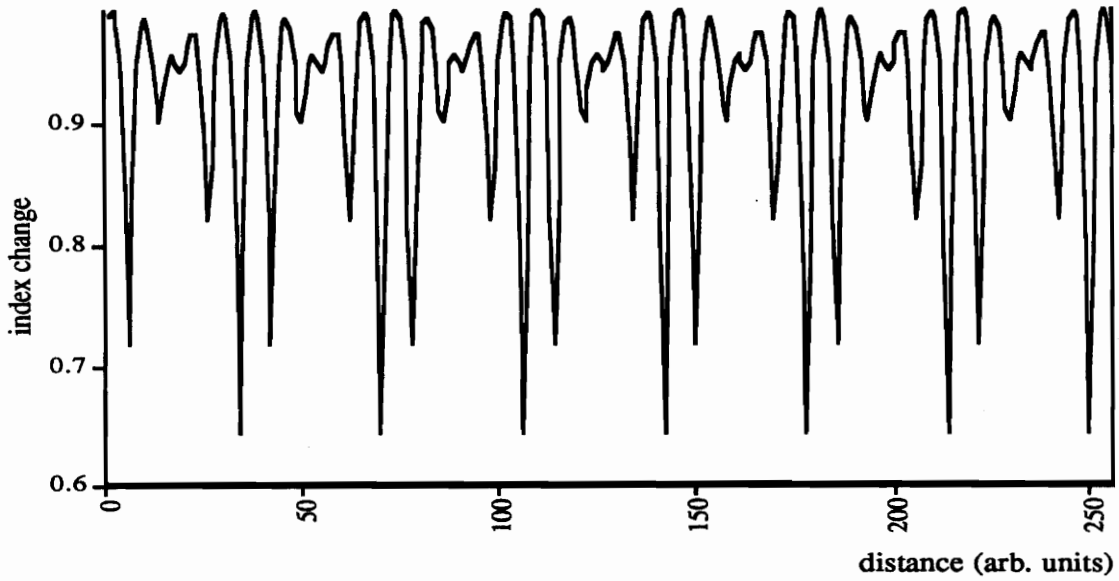

Figure 16. Normalized index of refraction change caused by the standing wave pattern in Figure 15. The amplitude of each standing wave has been assumed to be the inverse of the quantum efficiency.

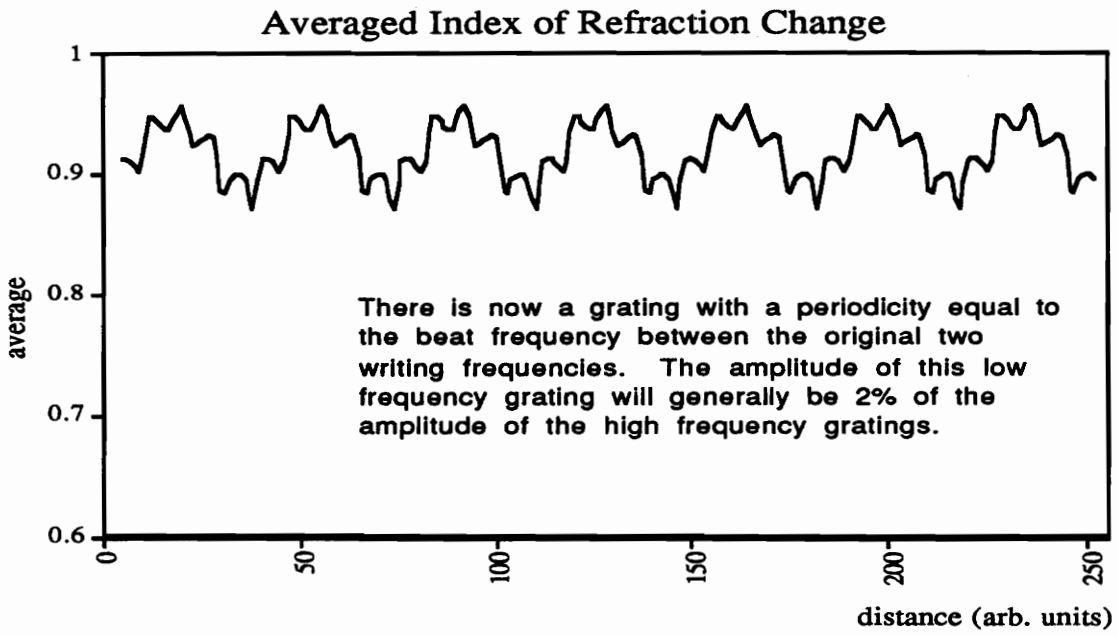

Figure 17. The index of refraction change over space, highlighting the creation of a beat frequency.

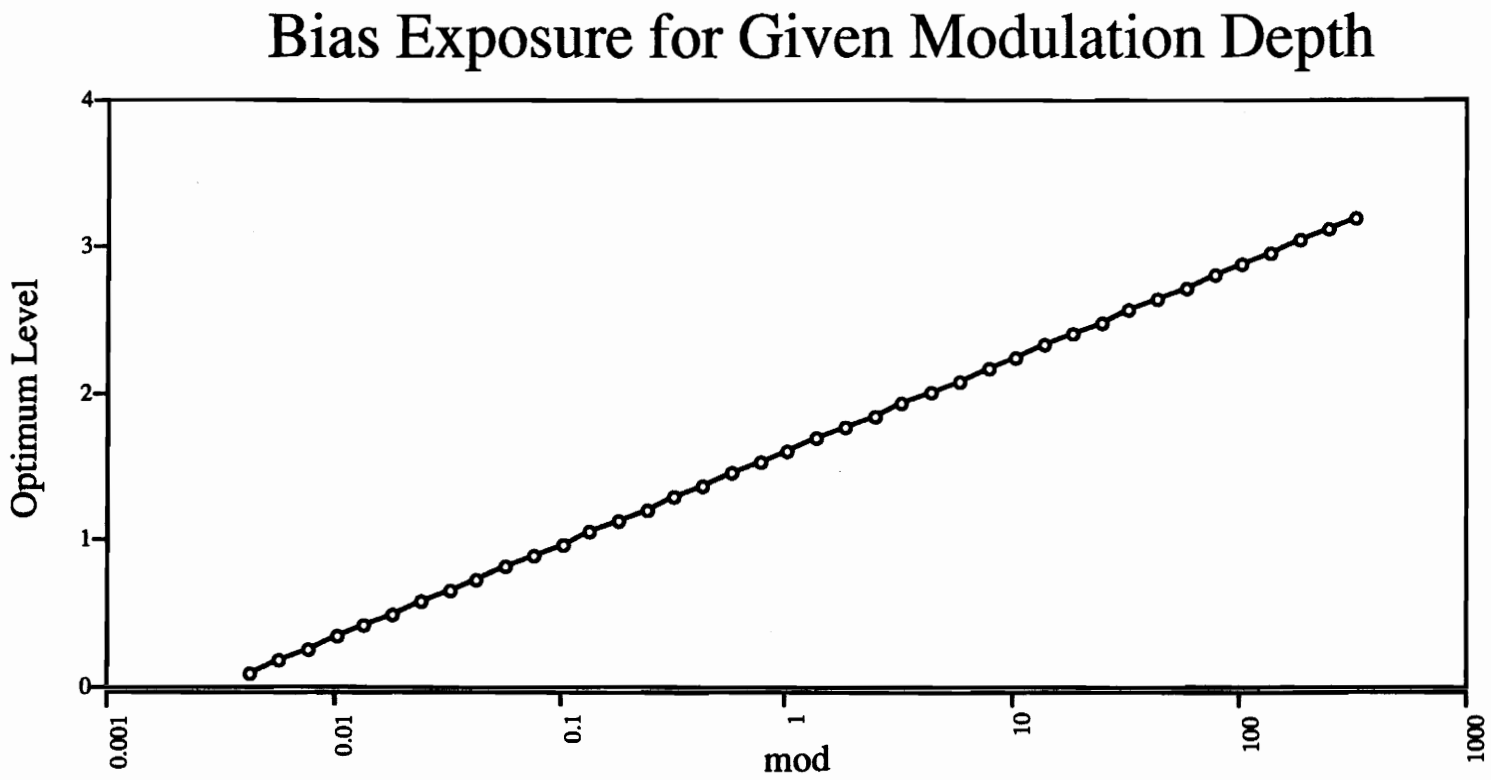

Figure 18. Optimum uniform exposure level normalized to the quantum efficiency. The writing wavelength powers have also been normalized to the quantum efficiency.

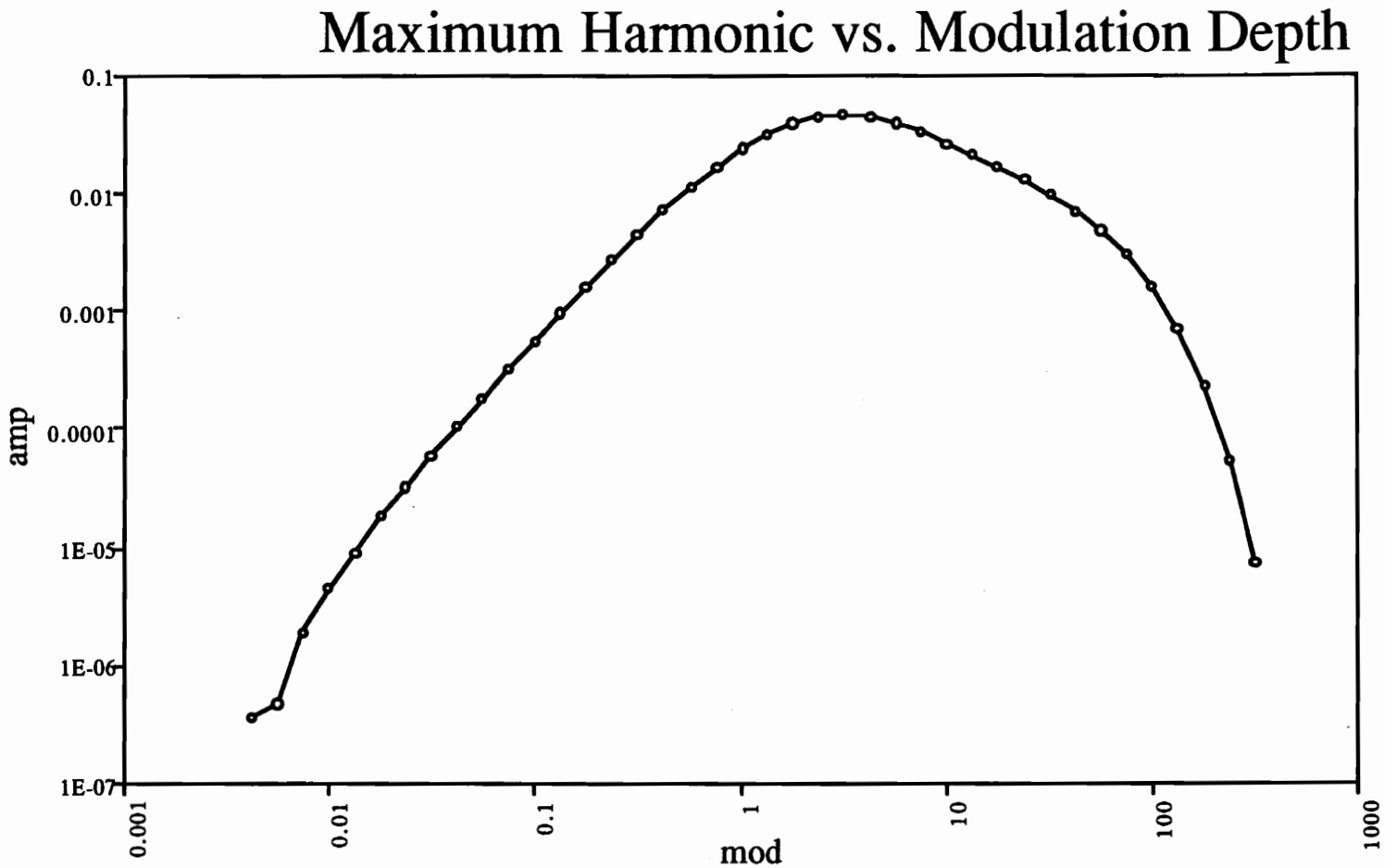

Figure 19Maximum beat frequency amplitude possible for a given modulation depth. The x-axis is the modulation depth normalized to the saturation level, and the y-axis is the amplitude of the resulting beat frequency grating normalized to the modulation depth. The modulation depths at each writing wavelength are assumed to be equal.

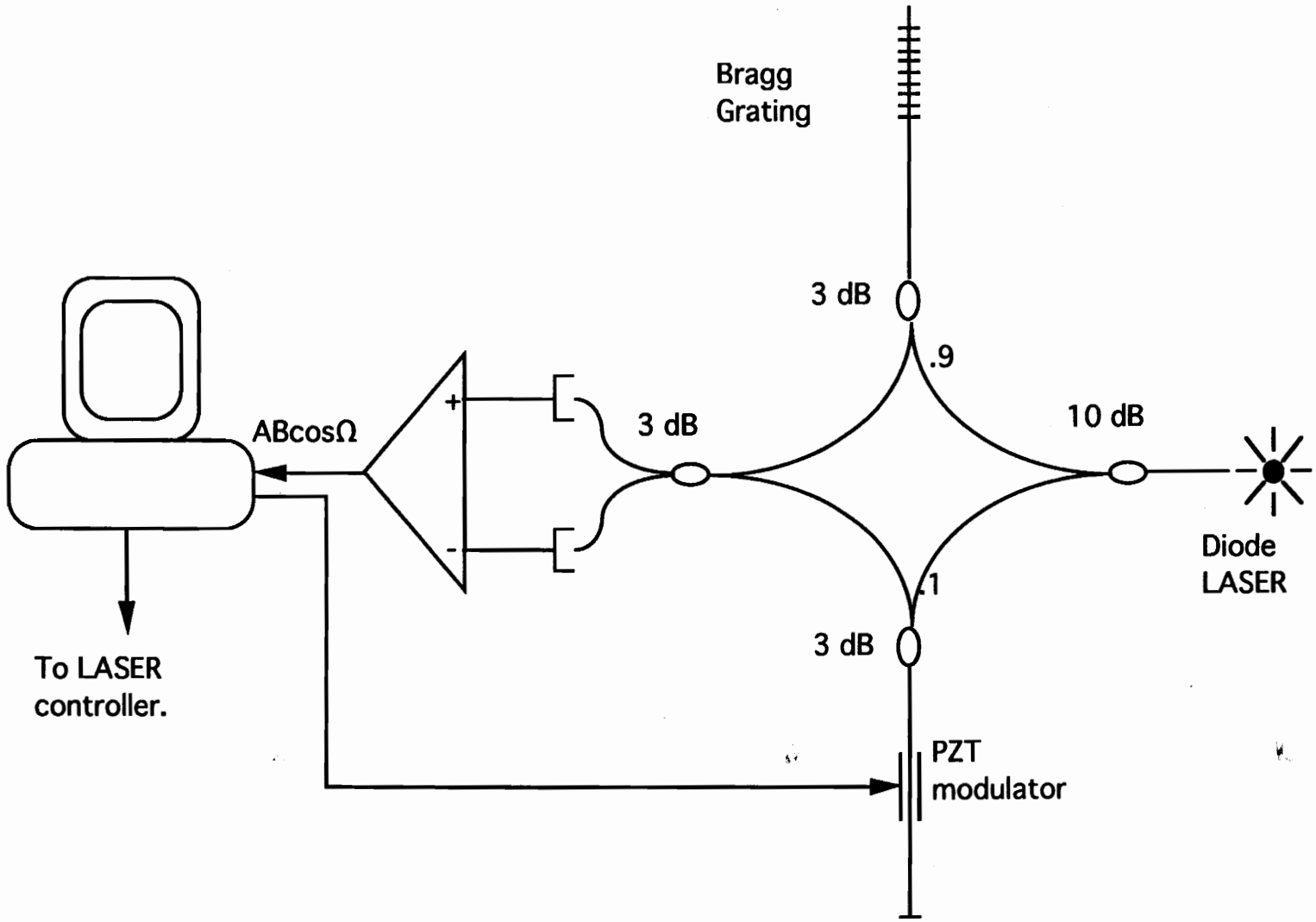

Figure 20. Experimental set-up to measure the vector reflection spectrum of a Bragg grating.

Mark Froggatt was born in Petersburg, Virginia on November 15, 1968. He attended Prince George Public schools through the eleventh grade, and entered Virginia Tech in the Fall of 1985. Mark entered the cooperative education program with NASA, Langley in Hampton, VA in March of 1987, thus delaying graduation by one year. In May of 1990, Mark graduated from Virginia Tech with a Bachelor of Science Degree in Electrical Engineering and began full-time work at Langley Research Center in the Nondestructive Evaluation Sciences Branch. Mark is currently working on the developement of fiber-optic sensor, and ultrasonic instrumentation.

Mark E. Froggatt